among patients with various renal diseases, those with ANCA-GN or HSPN showed a significantly higher tendency to be positive for HMGB1. In contrast, no significant relationship was found for the presence of anti-HMGB1 antibodies in the sera among patients with biopsy-proven renal diseases.

Logistic regression analysis showed that pathological diagnoses of ANCA-GN and HSPN were the factors associated with positive serum HMGB1. Even among patients undergoing renal biopsies – the population more likely to be serum HMGB1 positive than controls –, patients with ANCA-GN or HSPN are more likely to show positive serum HMGB1. In contrast, lupus nephritis did not show a tendency to be positive for serum HMGB1. Of interest was the fact that no significant association was observed between the presence of serum HMGB1 and other inflammatory parameters, including CRP, IL-1β, IL-6, and TNF-α [24]. The data in the present study suggest that in patients with renal disease HMGB1 is not simply a marker of inflammation in general but rather a marker of a more specific condition, such as vasculitis.

When patients with IgAN were further analyzed, glomerular crescent formation was associated with positive serum HMGB1. Since crescent formation is a well-known indicator of disease activity, HMGB1 may be related to the activity of IgAN. In addition, because IgAN is considered to be one form of vasculitis [26], the results also suggest that those who showed positive serum HMGB1 were more likely to have renal vasculitis, including ANCA-GN, HSPN, or active IgAN. For the purpose of comparison, we studied the expression of HMGB1 in the sera of patients with other nonrenal diseases. Four out of 5 patients with nonrenal vasculitis showed positive serum HMGB1 [unpubl. data]. Although the number of patients examined was too small to show any definite relationship, these data may support our current hypothesis that the presence or absence of serum HMGB1 is a key factor in understanding the pathology of vasculitis.

In our study, immunostaining for HMGB1 was performed on the kidney sections obtained from patients with ANCA-GN, HSPN, IgAN, or MCD. No positive staining was observed in the kidney specimens from MCD patients who were diagnosed with minor glomerular abnormalities. By contrast, in patients with ANCA-GN or IgAN, HMGB1 was strongly stained mainly in the macrophages of the interstitium, and staining was infrequently observed in the mononuclear cells in the glomeruli. The positive HMGB1 staining was observed regardless of the presence or absence of serum HMGB1. In other words, a discrepancy was noticed between the HMGB1 expression in the kidney and the presence or absence of HMGB1 in the sera. Therefore, it seems unlikely that the HMGB1 in the sera came mainly from the cells in the kidney. Rather, we assume that in patients with active vasculitis, including ANCA-GN, HSPN, or IgAN, serum HMGB1 was secreted from inflammatory cells [11, 12] or endothelial cells [27–30].

Concerning the role of HMGB1, relatively recent studies [31] have shown that HMGB1 released from the damaged organ acts to mobilize inflammatory cells and/or stem cells to the injured site, where they work to mediate tissue repair. In contrast, HMGB1 has also been shown to be harmful to organs when it is overly released [9–12]. Animal experiments revealed that HMGB1 can induce tissue damage in the lung [16], the joints [17], and the liver [18, 19]. We found that when purified HMGB1 protein was administered to the rat kidney, strong macrophage inflammation was observed in the interstitial area [unpubl. data]. Taking all these animal experiments together, we are considering the possibility that HMGB1 is expressed in sera-activated immune cells and accelerates renal diseases.

In summary, the present study demonstrated that HMGB1, a proinflammatory cytokine, is likely to be detected in sera of patients with biopsy-proven renal vasculitis, including ANCA-GN, HSPN, and IgAN with crescent formation. Further studies are needed to determine the pathological roles of HMGB1 in the kidney.

References

1 Paonessa G, Frank R, Cortese R: Nucleotide sequence of rat liver HMG1 cDNA. Nucleic Acids Res 1987;15:9077.

2 Ferrari S, Ronfani L, Calogero S, Bianchi ME: The mouse gene coding for high mobility group 1 protein (HMG1). J Biol Chem 1994;269:28803–28808.

3 Wen L, Huang JK, Johnson BH, Reeck GR: A human placental cDNA clone that encodes nonhistone chromosomal protein HMG-1. Nucleic Acids Res 1989;17:1197–1214.

4 Bustin M: Regulation of DNA-dependent activities by the functional motifs of the high-mobility-group chromosomal proteins. Mol Cell Biol 1999;19:5237–5246.

5 Hori O, Brett J, Slattery T, et al: The receptor for advanced glycation end products (RAGE) is a cellular binding site for amphoterin. Mediation of neurite outgrowth and co-expression of RAGE and amphoterin in the developing nervous system. J Biol Chem 1995;270:25752–25761.

6 Taguchi A, Blood DC, del Toro G, Canet A, Lee DC, Qu W, Tanji N, Lu Y, Lalla E, Fu C, Hofmann MA, Kislinger T, Ingram M, Lu A, Tanaka H, Hori O, Ogawa S, Stern DM, Schmidt AM: Blockade of RAGE-amphoterin signalling suppresses tumour growth and metastases. Nature 2000;405:354–360.
7 Fages C, Nolo R, Huttunen HJ, Eskelinen E, Rauvala H: Regulation of cell migration by amphoterin. J Cell Sci 2000;113:611–620.
8 Wang H, Bloom O, Zhang M, Vishnubhakat JM, Ombrellino M, Che J, Frazier A, Yang H, Ivanova S, Borovikova L, Manogue KR, Faist E, Abraham E, Andersson J, Andersson U, Molina PE, Abumrad NN, Sama A, Tracey KJ: HMG-1 as a late mediator of endotoxin lethality in mice. Science 1999;285:248–251.
9 Andersson U, Erlandsson-Harris H, Yang H, Tracey KJ: HMGB1 as a DNA-binding cytokine. J Leukoc Biol 2002;72:1084–1091.
10 Yang H, Wang H, Tracey KJ: HMG-1 rediscovered as a cytokine. Shock 2001;15:247–253.
11 Erlandsson Harris H, Andersson U: Mini-review: the nuclear protein HMGB1 as a proinflammatory mediator. Eur J Immunol 2004;34:1503–1512.
12 Wang H, Yang H, Tracey KJ: Extracellular role of HMGB1 in inflammation and sepsis. J Intern Med 2004;255:320–331.
13 Ombrellino M, Wang H, Ajemian MS, Talhouk A, Scher LA, Friedman SG, Tracey KJ: Increased serum concentrations of high-mobility-group protein 1 in haemorrhagic shock. Lancet 1999;354:1446–1447.
14 Taniguchi N, Kawahara K, Yone K, Hashiguchi T, Yamakuchi M, Goto M, Inoue K, Yamada S, Ijiri K, Matsunaga S, Nakajima T, Komiya S, Maruyama I: High mobility group box chromosomal protein 1 plays a role in the pathogenesis of rheumatoid arthritis as a novel cytokine. Arthritis Rheum 2003;48:971–981.
15 Hatada T, Wada H, Nobori T, Okabayashi K, Maruyama K, Abe Y, Uemoto S, Yamada S, Maruyama I: Plasma concentrations and importance of high mobility group box protein in the prognosis of organ failure in patients with disseminated intravascular coagulation. Thromb Haemost 2005;94:975–979.
16 Abraham E, Arcaroli J, Carmody A, Wang H, Tracey KJ: HMG-1 as a mediator of acute lung inflammation. J Immunol 2000;165:2950–2954.
17 Kokkola R, Sundberg E, Ulfgren AK, Palmblad K, Li J, Wang H, Ulloa L, Yang H, Yan XJ, Furie R, Chiorazzi N, Tracey KJ, Andersson U, Harris HE: High mobility group box chromosomal protein 1: a novel proinflammatory mediator in synovitis. Arthritis Rheum 2002;46:2598–2603.
18 Tsung A, Sahai R, Tanaka H, Nakao A, Fink MP, Lotze MT, Yang H, Li J, Tracey KJ, Geller DA, Billiar TR: The nuclear factor HMGB1 mediates hepatic injury after murine liver ischemia-reperfusion. J Exp Med 2005;201:1135–1143.
19 Watanabe T, Kubota S, Nagaya M, Ozaki S, Nagafuchi H, Akashi K, Taira Y, Tsukikawa S, Oowada S, Nakano S: The role of HMGB-1 on the development of necrosis during hepatic ischemia and hepatic ischemia/reperfusion injury in mice. J Surg Res 2005;124:59–66.
20 Uesugi H, Ozaki S, Sobajima J, Osakada F, Shirakawa H, Yoshida M, Nakao K: Prevalence and characterization of novel pANCA, antibodies to the high mobility group nonhistone chromosomal proteins HMG1 and HMG2, in systemic rheumatic diseases. J Rheumatol 1998;25:703–709.
21 Sobajima J, Ozaki S, Uesugi H, Osakada F, Shirakawa H, Yoshida M, Nakao K: Prevalence and characterization of perinuclear anti-neutrophil cytoplasmic antibodies (P-ANCA) directed against HMG1 and HMG2 in ulcerative colitis (UC). Clin Exp Immunol 1998;111:402–407.
22 Sobajima J, Ozaki S, Uesugi H, Osakada F, Inoue M, Fukuda Y, Shirakawa H, Yoshida M, Rokuhara A, Imai H, Kiyosawa K, Nakao K: High mobility group (HMG) non-histone chromosomal proteins HMG1 and HMG2 are significant target antigens of perinuclear anti-neutrophil cytoplasmic antibodies in autoimmune hepatitis. Gut 1999;44:867–873.
23 Yamada S, Inoue K, Yakabe K, Imaizumi H, Maruyama I: High mobility group protein 1 (HMGB1) quantified by ELISA with a monoclonal antibody that does not cross-react with HMGB2. Clin Chem 2003;49:1535–1537.
24 Yamada S, Yakabe K, Ishii J, Imaizumi H, Maruyama I: New high mobility group box 1 assay system. Clin Chim Acta 2006;372:173–178.
25 Taylor WE, Bhasin S, Artaza J, Byhower F, Azam M, Willard DH Jr, Kull FC Jr, Gonzalez-Cadavid N: Myostatin inhibits cell proliferation and protein synthesis in C2C12 muscle cells. Am J Physiol Endocrinol Metab 2001;280:E221–E228.
26 Davin JC, Ten Berge IJ, Weening JJ: What is the difference between IgA nephropathy and Henoch-Schönlein purpura nephritis? Kidney Int 2001;59:823–834.
27 Degryse B, Bonaldi T, Scaffidi P, Müller S, Resnati M, Sanvito F, Arrigoni G, Bianchi ME: The high mobility group (HMG) boxes of the nuclear protein HMG1 induce chemotaxis and cytoskeleton reorganization in rat smooth muscle cells. J Cell Biol 2001;152:1197–1206.
28 Mullins GE, Sunden-Cullberg J, Johansson AS, Rouhiainen A, Erlandsson-Harris H, Yang H, Tracey KJ, Rauvala H, Palmblad J, Andersson J, Treutiger CJ: Activation of human umbilical vein endothelial cells leads to relocation and release of high-mobility group box chromosomal protein 1. Scand J Immunol 2004;60:566–573.
29 Reinhart K, Bayer O, Brunkhorst F, Meisner M: Markers of endothelial damage in organ dysfunction and sepsis. Crit Care Med 2002;30(5 Suppl):S302–S312.
30 Bradley JR, Lockwood CM, Thiru S: Endothelial cell activation in patients with systemic vasculitis. QJM 1994;87:741–745.
31 Palumbo R, Sampaolesi M, De Marchis F, Tonlorenzi R, Colombetti S, Mondino A, Cossu G, Bianchi ME: Extracellular HMGB1, a signal of tissue damage, induces mesoangioblast migration and proliferation. J Cell Biol 2004;164:441–449.

NEC915.indd 8 24.01.2008 10:39:31

Delayed Postischemic Treatment With Fluvastatin Improved Cognitive Impairment After Stroke in Rats

Munehisa Shimamura, MD, PhD; Naoyuki Sato, MD, PhD; Masataka Sata, MD, PhD; Hitomi Kurinami, MD; Daisuke Takeuchi, MD; Kouji Wakayama, MD; Takuya Hayashi, MD, PhD; Hidehiro Iida, MD, PhD; Ryuichi Morishita, MD, PhD

Background and Purposes—Recent clinical evidences indicate that statins may have beneficial effects on the functional recovery after ischemic stroke. However, the effect of delayed postischemic treatment with statins is still unclear. In the present study, we evaluated the effects of fluvastatin in the chronic stage of cerebral infarction in a rat model.

Methods—Rats exposed to permanent middle cerebral artery occlusion were treated for 3 months with fluvastatin beginning from 7 days after stroke. MRI, behavioral analysis, and immunohistochemistry were performed.

Results—Two months of treatment with fluvastatin showed the significant recovery in spatial learning without the decrease in serum total cholesterol level and worsening of infarction. Microangiography showed a significant increase in capillary density in the peri-infarct region in fluvastatin-treated rats after 3 months of treatment. Consistently, BrdU/CD31-positive cells were significantly increased in fluvastatin-treated rats after 7 days of treatment. MAP1B-positive neurites were also increased in the peri-infarct region in fluvastatin-treated rats. In addition, rats treated with fluvastatin showed the reduction of superoxide anion after 7 days of treatment and the reduction of Aβ deposits in the thalamic nuclei after 3 months of treatment.

Conclusions—Thus, delayed postischemic administration of fluvastatin had beneficial effects on the recovery of cognitive function without affecting the infarction size after ischemic stroke. Pleiotropic effects of fluvastatin, such as angiogenesis, neuritogenesis, and inhibition of superoxide production and Aβ deposition, might be associated with a favorable outcome. (***Stroke*. 2007;38:3251-3258.**)

Key Words: angiogenesis ■ cerebral infarct ■ microcirculation ■ statins

Despite conflicting data correlating cholesterol level with stroke, 2 early trials of HMG-CoA reductase inhibitors (statins) in patients after myocardial infarction patients showed a reduction in stroke risk as a secondary end point.[1] A meta-analysis of 9 statin intervention trials, which enrolled patients with coronary artery disease or those at high risk for coronary disease, demonstrated a 21% relative risk reduction for stroke after 5 years of treatment.[2] Another clinical evidence suggests that the commencement of statins within 4 weeks of a stroke results in a favorable 90-day outcome.[3] To clarify the effects of postischemic statin treatment, previous studies in which atorvastatin was started 1 day after stroke in rodents showed improvement of sensory motor deficit through induction of angiogenesis, neurogenesis, and synaptogenesis.[4,5] These pleiotropic effects of statins were shown to be the result of induction of vascular endothelial growth factor or brain-derived neurotrophic factor.[4] Additionally, the microvascular dysfunction in the posttreatment of stroke with recombinant human tissue-type plasminogen activator could be reduced by statins in rodent model.[6] However, the effect of delayed treatment with statins after ischemic stroke is still unknown. From this viewpoint, we investigated whether chronic statin treatment beginning 7 days after ischemic stroke had influences on neurological deficits and pathophysiology after the permanent middle cerebral artery occlusion (MCAo) model in rats.

Materials and Methods

Surgical Procedure

Male Wistar rats (270 to 300 grams; Charles River; Kanagawa, Japan) were used in this study. The right MCA was occluded by placement of poly-L-lysine–coated 4-0 nylon, as described previously.[7]

Protocol for Treatment and Behavioral Tests

Ten rats were only anesthetized (sham operation) and 32 rats were subjected to MCAo (day 1). Based on neuromuscular function on day 7, the rats were divided equally into saline-treated (n=16) or fluvastatin-treated (n=16) groups. Fluvastatin (5 mg/kg per day;

Received February 14, 2007; final revision received April 27, 2007; accepted May 30, 2007.

From Department of Advanced Clinical Science and Therapeutics (M.S., M.Sata, K.W.), Graduate School of Medicine, the University of Tokyo, Japan; Department of Clinical Gene Therapy (N.S., H.K., D.T., R.M.), Graduate School of Medicine, Osaka University, Japan; Department of Investigative Radiology (T.H., H.I.), National Cardiovascular Center, Research Institute, Japan.

Correspondence to Ryuichi Morishita, MD, PhD, Professor, Division of Clinical Gene Therapy, Graduate School of Medicine, Osaka University, 2-2 Yamada-oka, Suita 565-0871, Japan. E-mail morishit@cgt.med.osaka-u.ac.jp

© 2007 American Heart Association, Inc.

Stroke is available at http://stroke.ahajournals.org

DOI: 10.1161/STROKEAHA.107.485045

provided by Novartis Pharma) or saline was given by gavage from day 7 to 100. We chose the dose (5 mg/kg per day), because a previous report showed that this dose could effectively induce angiogenesis in ischemic limb.[8] On day 55, neuromuscular function and locomotor activity were evaluated in the surviving rats. Then, cognitive function was examined by Morris water maze from day 56 to 63, because the effects of neuronal regeneration could be detected not in the early stage but in the chronic stage of ischemic brain such as 49 to 53 days after the insult.[9] On day 96, MRI was performed. On day 100, microangiography was performed.

MRI

High-resolution T1-weighted fast spin echo sequence images (repetition time [TR]=1500 ms; echo time [TE]=10.3 ms; field of view [FOV]=4× 3 cm; matrix=256×192; slice thickness=1.5 mm; slice gap=0.5 mm; number of slices=16; number of excitation=10; total time=9.39 min) were obtained using a 3-T MRI scanner (Signa LX VAH/I; GE).

Sensory Motor Deficit and Locomotor Activity

Although there are various batteries for testing sensory motor deficit, we used a simple protocol.[10] For forelimb flexion, rats were held by the tail on a flat surface. Paralysis of the forelimbs was evaluated by the degree of left forelimb flexion. For torso twisting, rats were held by the tail on a flat surface. The degree of body rotation was checked. For lateral push, rats were pushed either left or right. Rats with right MCA occlusion showed weak or no resistance against a left push. For hind limb placement, one hind limb was removed from the surface. Rats with right MCA occlusion showed delayed or no replacement of the hind limb when it was removed from the surface.

Spontaneous activity was measured via the open field (0.69 m^2). We set the sensor, which also put beams on the field, at 30 cm above the field. The number of count, which is when the animal crosses the beam, was measured for 30 minutes.

Morris Water Maze Task

A cylindrical tank 1.5 m in diameter was filled with water (25°C), and a transparent platform 15 cm in diameter was placed at a fixed position in the center of 1 of the 4 quadrants (O'Hara & Co, Ltd). In the hidden platform trials, we performed the tests 4 times per day for 4 days. When the rat could not reach the platform, the latency was set at 60 sec. In the visible platform trials, the tests were performed 4 times per day for 4 days. The acquired data were averaged per day.

Evaluation of Capillary Density

Using a recently developed microangiographic technique,[11] capillary density and blood–brain barrier leakage were evaluated in the cerebral cortex after MCA occlusion. The area or length of vessels was analyzed with an angiogenesis image analyzer (version 1.0; Kurabo).

Immunohistochemical Study: Bromodeoxyuridine Labeling

To identify newly formed DNA, saline-treated (n=5) and fluvastatin-treated (n=5) rats received injections of bromodeoxyuridine (BrdU, 50 mg/kg; Sigma-Aldrich, Saint Louis, Mo) intraperitoneally starting on day 7 twice per day until day 13. Rats were euthanized on day 14. After the sections (8-μm thickness) was fixed in 10% formaldehyde/MeOH neutral buffer solution and blocked, they were incubated with mouse monoclonal anti-rat CD31 antibody (1:100; BD Biosciences; San Jose, Calif), goat polyclonal anti-doublecortin (anti-DCX; Santa Cruz) antibody (1:100; Santa Cruz, Calif), mouse monoclonal anti-NeuN antibody (1:1000; Chemicon, Temecula, Calif), or mouse monoclonal anti-MAP1B antibody (1:100; Sigma-Aldrich), followed by anti-mouse goat fluorescent antibody (1:1000 for NeuN and MAP1B, 1:400 for CD31, Alexa Flour 546, Molecular Probes; Eugene, Ore) or anti-goat donkey fluorescent antibody (1:1000 for DCX Alexa Fluor 546). For double immunostaining, these sections were fixed again and incubated in 2 N HCl at 37°C for 30 minutes. After blocking, they were incubated with rat monoclonal anti-BrdU antibody (1:200; Abcam, Cambridge, UK) followed by anti-rat goat fluorescent antibody (1:1000, Alexa Fluor 488). For immunohistochemical staining for Aβ, sections were pretreated for 30 minutes with hot (85°C) citrate buffer as described before.[12] Confocal images were acquired using an FV-300 (Olympus).

Table. Infarction Volume Calculated by MRI, Blood Pressure, and Serum Total Cholesterol

	Sham	MCAo+S	MCAo+F	*P*
Infarction volume in total rats (mm^3)	...	283.8±23.9	278.4±26.4	0.851
Type of infarction in Figure 1a (N of rats)				0.828
A	...	12	11	...
B	...	3	3	...
C	...	1	2	...
Infarction volume (mm^3) in type A rats	...	322.8±15.0	327.0±18.8	0.758
Systolic blood pressure (mm Hg) in type A rats				
Day 7	116.1±5.4	123.7±6.0	115.5±7.3	0.654
Day 56	146.5±4.7	148.3±2.7	136.1±5.2	0.132
Serum total cholesterol (mg/dl) in type A rats on day 56	85.9±5.6	75.3±3.5	73.5±2.7	0.949

Type A, low-intensity area seen in the dorsolateral and lateral portions of the neocortex and the entire caudate putamen; type B, low-intensity area seen in the dorsolateral and lateral portions of the neocortex and in part of the caudate putamen; type C, low-intensity area seen in part of the lateral neocortex and caudate putamen. MCAo+S, saline-treated rats after MCAo; MCAo+F, fluvastatin-treated rats after MCAo.

P, saline vs fluvastatin.

Quantitative Histological Analysis

To quantify the immunoreactivity for MAP1B and Aβ, the acquired image was analyzed by Image J (version 1.32; NIH).

Detection of Superoxide Anion in Brain Sections

Superoxide anion was detected on day 14 as described previously.[13] Because intact cortex showed red fluorescence, we calculated the ratio of fluorescence as follows: ratio of fluorescence=[fluorescence intensity in ischemic core or peri-infarct region]/[fluorescence intensity in intact region].

Statistical Analysis

All values are expressed as mean±SEM. To analyze the differences in the type of cerebral infarction, χ^2 test was performed. The latency, path length, and mean speed in Morris water maze and sensory motor deficits were analyzed by a 2-factor repeated-measure ANOVA. Post hoc analyses were performed, and the Scheffe test was applied to control the inflation in type I error. The value of the serum total cholesterol, the blood pressure, and the spontaneous activity was analyzed by Scheffe rules. The differences in the immunohistochemistry and the volume of infarction were assessed by Mann–Whitney *U* analyses. In all cases, $P<0.05$ was considered significant.

Results

Effects of Fluvastatin on Cognitive Impairment

To confirm the severity of cerebral infarction, all rats were examined by T1-weighted MRI after 89 days of treatment. Although the total volume of infarction calculated in T1-weighted images was not different between rats treated with

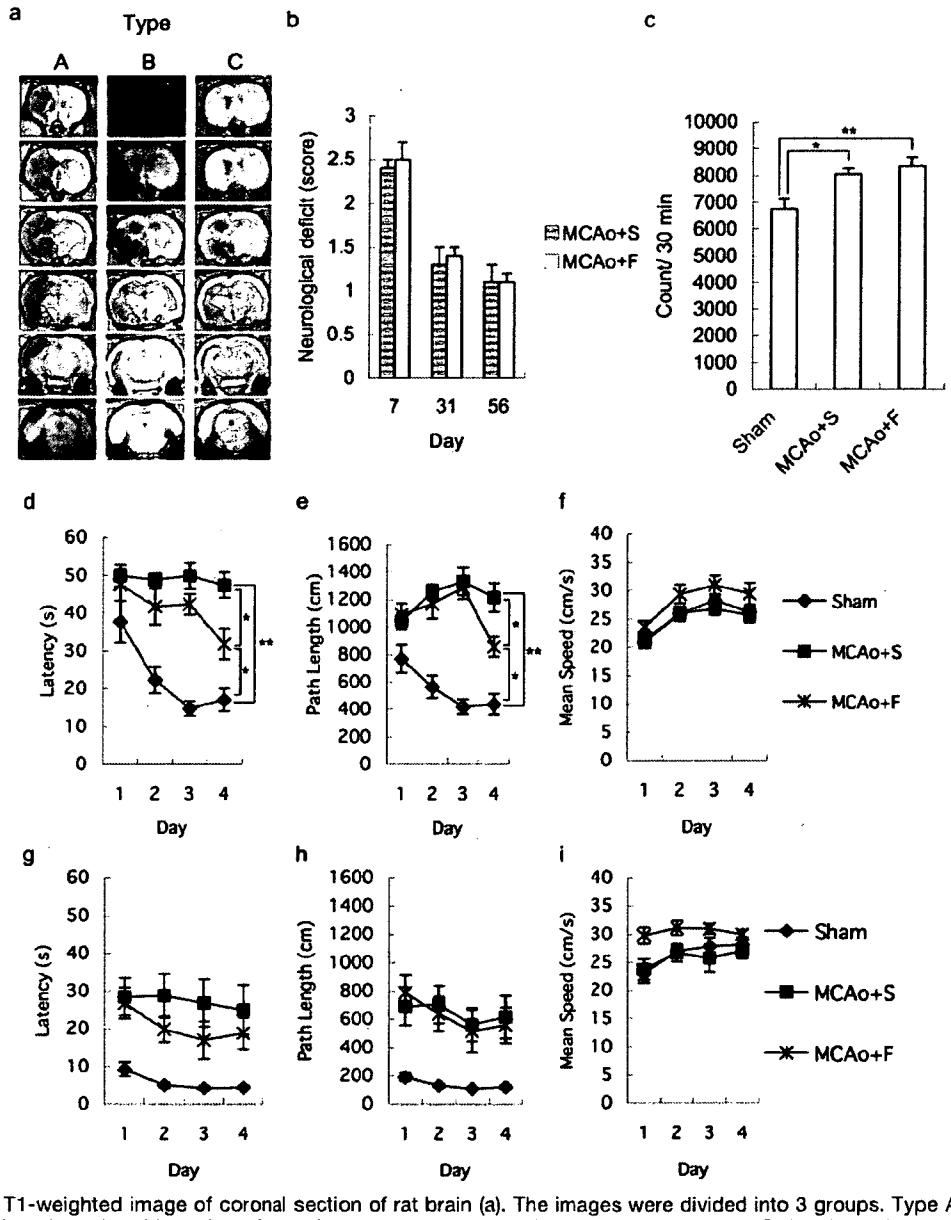

Figure 1. Typical T1-weighted image of coronal section of rat brain (a). The images were divided into 3 groups. Type A, low-intensity area seen in the dorsolateral and lateral portions of neocortex and the entire caudoputamen; type B, low-intensity area seen in the dorsolateral and lateral portions of neocortex and in part of the caudatoputamen; and type C, high-intensity area seen in part of the lateral neocortex and caudatoputamen. Sensory motor deficit (b). Spontaneous locomotor activity (c). Hidden platform test in Morris water maze. Each figure showed latency (d), path length (e), and mean speed (f). Days 1 to 4 indicate the trial day in the hidden platform test (56 to 59 days after middle cerebral artery occlusion). Visible platform test in Morris water maze. Each figure showed latency (g), path length (h), and mean speed (i). Days 1 to 4 indicate the day in the visible platform test (60 to 63 days after middle cerebral artery occlusion). MCAo+S indicates rats treated with saline after middle cerebral artery occlusion; MCAo+F, rats treated with fluvastatin after middle cerebral artery occlusion.

saline and fluvastatin (Table), the pattern of cerebral infarction was divided into 3 groups: type A, low-intensity area seen in the dorsolateral and lateral portions of the neocortex and the entire caudate putamen; type B, low-intensity area seen in the dorsolateral and lateral portions of the neocortex and in part of the caudate putamen; type C, low-intensity area seen in part of the lateral neocortex and caudate putamen (Figure 1a). In type C, most of the lateral neocortex was intact. To exclude the influence of the pattern of cerebral infarction on cognitive function, we focused on type A rats in the present study. The volume of cerebral infarction in type A rats was not different between the groups (Table). Blood pressure and serum total cholesterol also showed no difference among the groups (Table).

Sensory motor deficit had spontaneously recovered to some extent by 8 weeks in both groups, and there was no difference (Figure 1b). Locomotor activity in rats subjected to MCAo was increased as compared with that in sham-operated rats, as described before,[14] but there was no significant difference between fluvastatin-treated and saline-treated rats (Figure 1c). In Morris water maze (Figure 1d-i), which examines spatial learning, there were significant differences

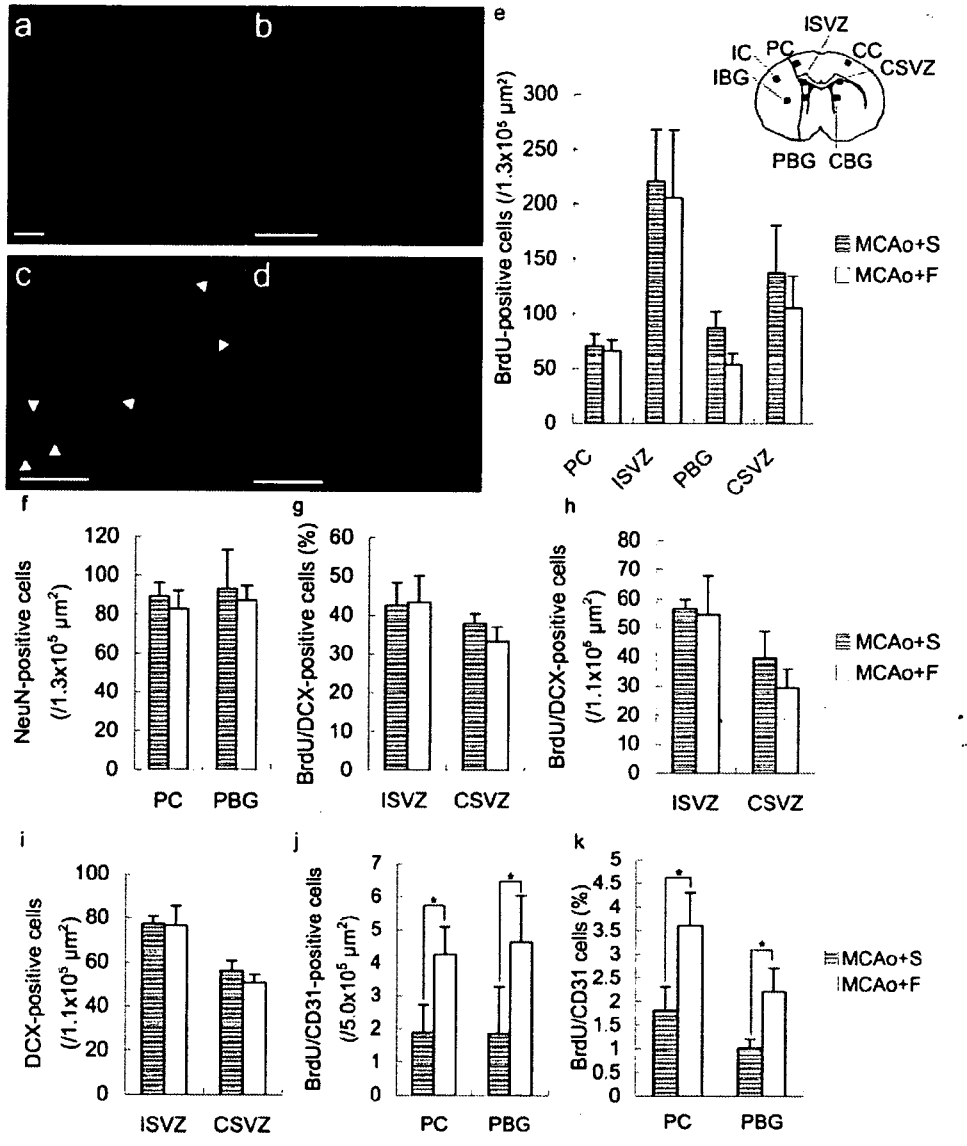

Figure 2. Representative images of immunohistochemical staining on day 14. Rats treated with fluvastatin (a through c), rats treated with saline (d). Although BrdU-positive cells were observed in the peri-infarct cortex (a), peri-infarct basal ganglia, and subventricular zone, these cells did not express NeuN (a), but expressed DCX in the subventricular zone (b). Fluvastatin-treated rats showed some BrdU/CD31-positive cells (arrows, c), although most BrdU-positive cells were negative for CD31 in saline-treated rats (d). The number of BrdU-positive cells (e), NeuN-positive cells (f), BrdU/DCX-positive cells (h), DCX-positive cells (i), and BrdU/CD31-positive cells (j); the percentage of BrdU/DCX-positive cells (g) or BrdU/CD31 cells (k) in total BrdU-positive cells. PC indicates peri-infarct cortex; PBG, peri-infarct basal ganglia; IC, infarcted cortex; IBG, ischemic basal ganglia; ISVZ, subventricular zone on infarcted side; CC, contralateral cortex, CSVZ, subventricular zone on contralateral side; CBG, contralateral basal ganglia (n=5 in each group, $^*P<0.05$, bar=100 μm).

in the latency and path length in hidden platform test among the groups (supplemental Table I, available online at http://stroke.ahajournals.org). A significant difference was observed on day 4 between fluvastatin-treated and saline-treated rats (supplemental Table I). Also, there was a significant difference between sham and saline-treated rats (supplemental Table I). There was no significant difference both in swimming speed and visible platform test, which excluded the possible influence of visual loss, sensory motor deficit, and motivation on the results.[15] These data suggest that impaired spatial learning was improved by fluvastatin.

Histological Changes by Fluvastatin

Next, we studied whether fluvastatin had some influences on the histology. Initially, we focused on neurogenesis and angiogenesis. To examine neurogenesis, we measured BrdU-incorporated cells after injecting BrdU from day 7 to day 13. Although BrdU-positive cells were observed in the subventricular zone and peri-infarct region (Figure 2a to 2d), the total number did not differ between the groups (Figure 2e). Similarly, the density of NeuN-positive cells, as a marker of adult neurons, also did not differ between the groups (Figure 2f), whereas there were no BrdU/NeuN-positive cells in the

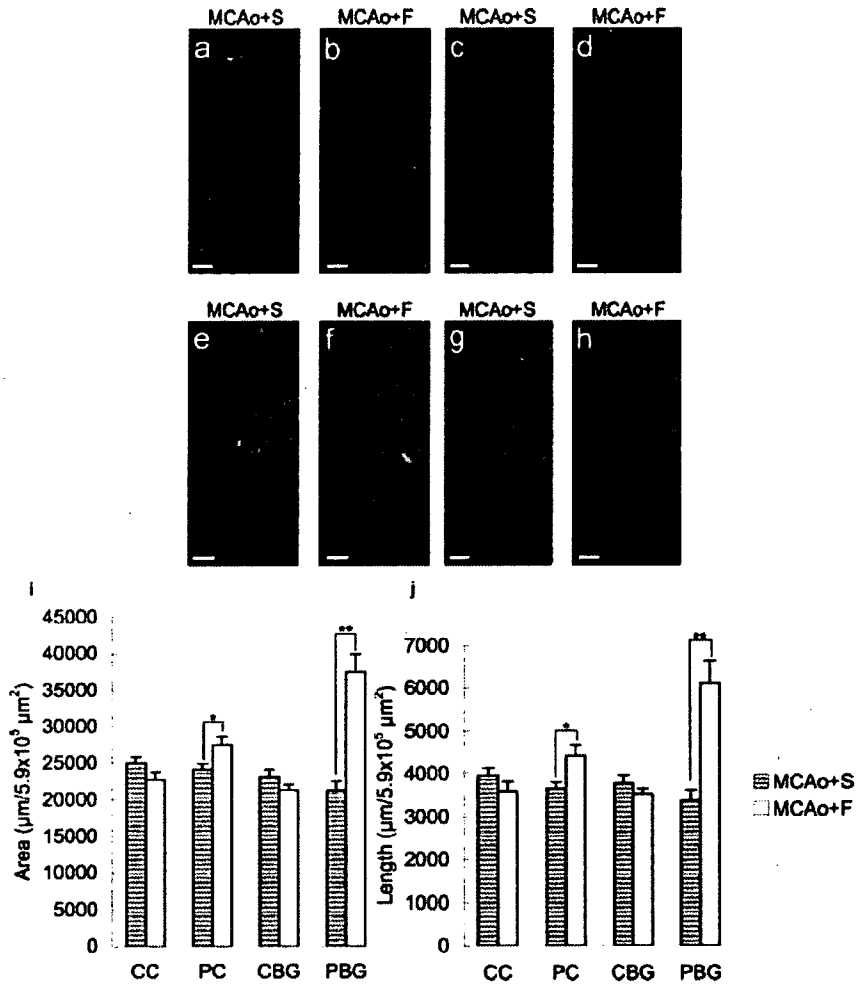

Figure 3. Microangiographic images using albumin-fluorescence isothiocyanate on day 100: (a and b) peri-infarct cortex; (c and d) contralateral cortex; (e and f) peri-infarct basal ganglia; (g and h) contralateral basal ganglia (bar=100 μm). Quantitative analysis (i and j) of microangiography. Rats treated with fluvastatin showed increased microvessels in the peri-infarct region (n=4 in each group, $^{*}P<0.05$, $^{**}P<0.01$).

peri-infarct cortex and subventricular zone (Figure 2a). Although some BrdU-positive cells expressing DCX, a marker for migrating neuroblasts, could be detected in subventricular zone (Figure 2b), the percentage in total BrdU-positive cells (Figure 2g) and the number (Figure 2h) did not differ between the groups. Also, the number of DCX-positive cells was same in the both groups (Figure 2i). There were no BrdU-positive cells expressing DCX in the cerebral cortex. Unexpectedly, these data suggest that neurogenesis was not enhanced by fluvastatin.

Thus, we further examined whether angiogenesis was affected by fluvastatin. In the peri-infarct cortex and basal ganglia, BrdU-positive cells that were positive for CD31 as a marker of endothelial cells could be detected (Figure 2c,2d). The number of BrdU/CD31-double-positive cells was significantly increased in fluvastatin-treated rats (Figure 2j). The percentage of BrdU/CD31-double-positive cells in total BrdU-positive cells was also increased in fluvastatin-treated rats (Figure 2k). Consistently, microangiography using FITC-conjugated albumin[11] also showed that microvessels were significantly increased in fluvastatin-treated rats only in the peri-infarct cortex and basal ganglia, without destruction of the blood–brain (Figure 3a to 3h). Quantitative analysis showed that the length and area of microvessels were also increased in the peri-infarct region, but not in the contralateral cortex and contralateral basal ganglia, in rats treated with fluvastatin, at 3 months after stroke (Figure 3i,j).

Because recent reports showed that neurite outgrowth was observed in the peri-infarct region from 7 to 14 days after cerebral infarction,[16,17] we next examined the effect of fluvastatin on neurite outgrowth. Immunohistochemical staining showed that treatment with fluvastatin significantly increased the immunoreactivity of MAP1B, a marker of neurite outgrowth, in neurites[16,18] (Figure 4), although the number of MAP1B-positive cells was the same in both groups. These data implied that the fluvastatin might promote angiogenesis, resulting in improvement of the microcirculation, and neurite outgrowth.

One possible explanation for the enhanced angiogenesis and neurite outgrowth is a decrease in oxidative stress by fluvastatin. To assess oxidative stress, we evaluated superoxide production using dihydroethidium staining (Figure 5a to 5e). Superoxide anion was increased in the ischemic core as compared with the contralateral region at 2 weeks after MCA occlusion (Figure 5a,5c). However, rats treated with fluvastatin showed a significant reduction in superoxide anion especially in the ischemic core region, but not in the peri-infarct cortex and basal ganglia (Figure 5b,5d,5e).

Finally, we examined Aβ deposition in the thalamic nuclei, because previous reports showed that Aβ deposits in the

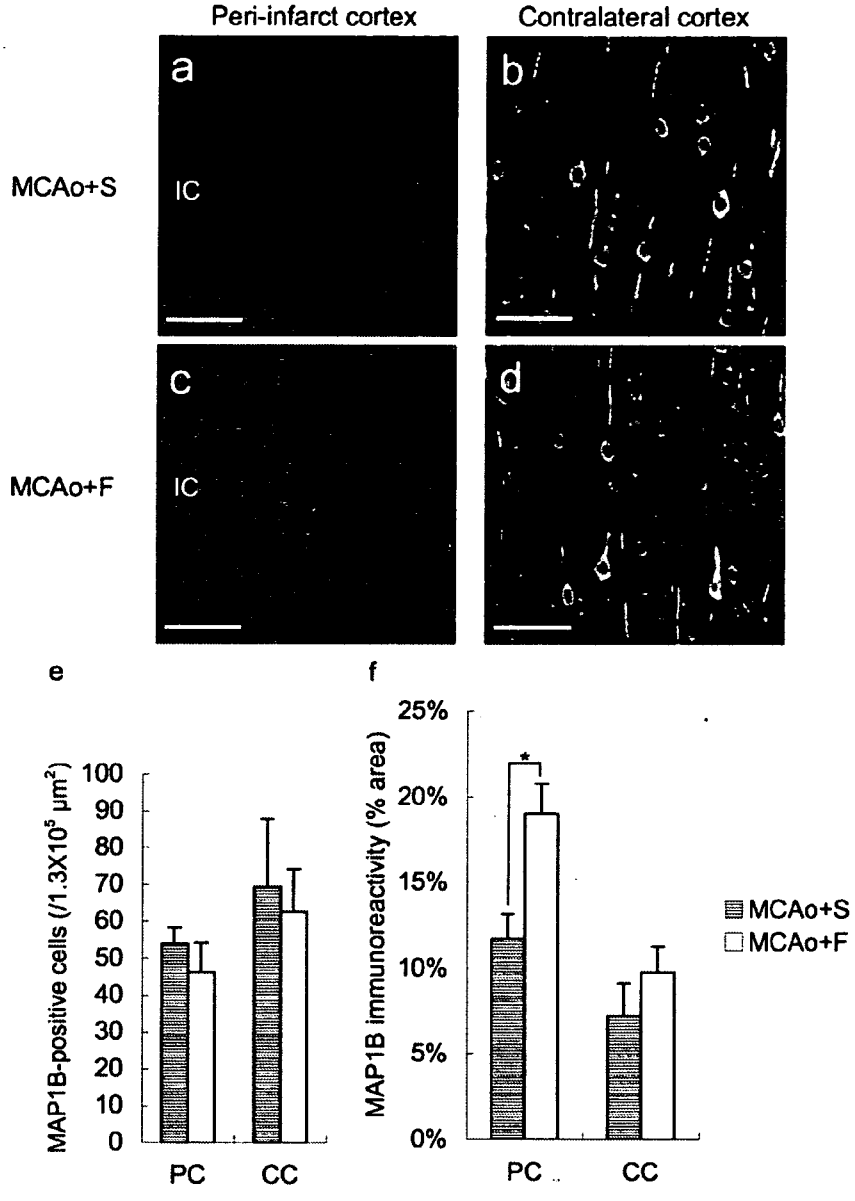

Figure 4. Typical images of immunohistochemical staining for MAP1B in peri-infarct cortex (a and c) and contralateral cortex (b and d) on day 14 (bar=100 μm). Although the number of MAP1B-positive cells was the same in both groups (e), immunoreactivity was higher in the peri-infarct region in fluvastatin-treated rats (f) (n=4 in each group, *$P<0.05$).

thalamic nuclei persisted as long as 9 months after focal cerebral ischemia.[12] Although immunohistochemical staining showed marked deposition of Aβ in the ventrolateral and ventromedial thalamic nuclei at 3 months after stroke, the area of Aβ deposits was significantly decreased in fluvastatin-treated rats (Figure 5f to 5h). In other regions, such as cortex or basal ganglia, there was no Aβ deposits in both groups as reported before.[12]

Discussion

Although several laboratories have shown that long-term pretreatment with a statin reduces infarct size in rodents,[19] no articles have reported the effects of delayed postischemic treatment with statins. The present study demonstrated that statin treatment beginning 7 days after ischemic stroke resulted in significant improvement of spatial learning at 8 weeks after stroke, without any change in the plasma cholesterol level and infarct size.

Fluvastatin-treated rats showed a significant increase of MAP1B in neurites in the peri-infarct region. Considering that MAP1B is especially prominent in extending neurites[20] and related to functional recovery after ischemic stroke,[17] one of the possible effects of fluvastatin is to enhance neurite outgrowth, "neuritogenesis," in the early stage of treatment. This speculation might be supported by the recent study demonstrating that neurite outgrowth is accelerated by pravastatin via inhibiting the activity of geranylgeranylated proteins such as RhoA.[21]

As BrdU/CD31-positive cells were increased 14 days after MCAo and microvessels were also increased in the peri-infarct region 100 days after MCAo, fluvastatin enhanced angiogenesis and resulted in improvement of microcirculation in the peri-infarct region. Although the relationship between the improved microcirculation and behavior is still unclear, a recent report demonstrated that the restoration of perfusion by collateral growth and new capillaries in the

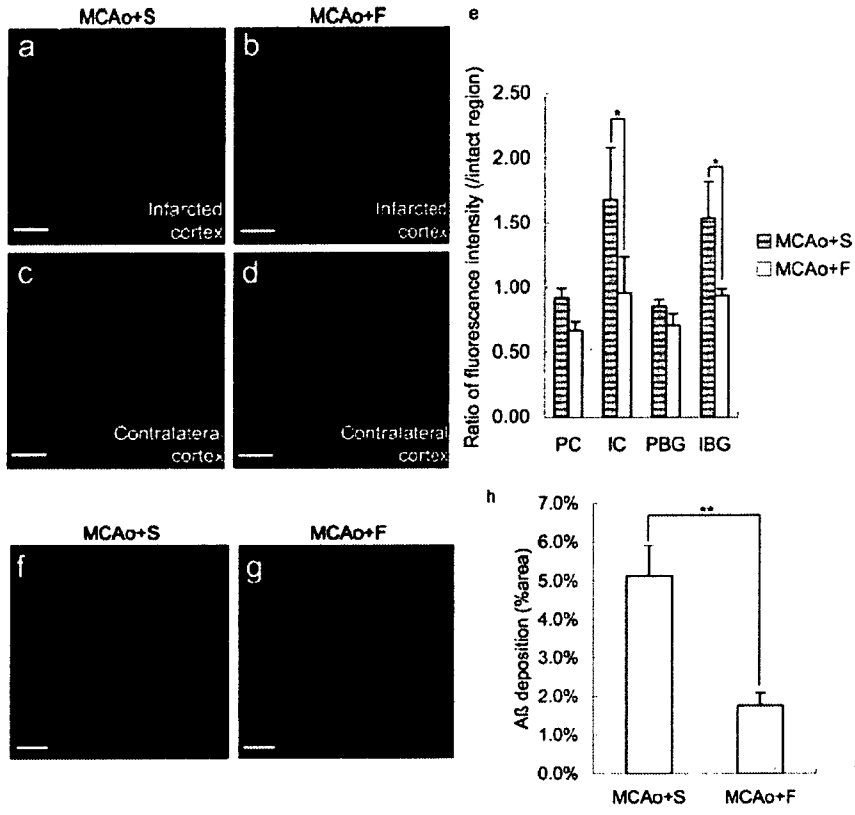

Figure 5. a through e, Superoxide anion detected by dihydroethidium staining on day 14. Red spots show the existence of superoxide anion. Fluorescence intensity was higher in the infarcted cortex (a) compared with the contralateral cortex (c). Fluvastatin-treated rats showed decreased fluorescence intensity in the infarcted cortex (b), although there was no difference in the peri-infarct cortex and basal ganglia (e) (n=4 in each group, $^{*}P<0.05$, bar=100 μm). Deposition of Aβ in thalamus on day 100 after middle cerebral artery occlusion. Although deposition of Aβ was observed in the thalamic nuclei (f and g), there was no deposition in other regions such as the cortex and basal ganglia. Quantitative analysis showed decreased Aβ deposition in fluvastatin-treated rats (h) (n=6 in each group, $^{**}P<0.01$, bar=200 μm).

ischemic border zone around a cortical infarct supported long-term functional recovery in rats.[22] Additionally, others reported that some patients who received tissue plasminogen activator therapy with no immediate clinical improvement despite early recanalization showed delayed clinical improvement.[23] From these viewpoints, it is likely that the improvement of microcirculation is an important factor for the functional recovery.

Of importance, fluvastatin reduced deposition of Aβ in the ventrolateral–ventromedial thalamic nuclei in the chronic stage of ischemic stroke, although rats subjected to focal cerebral ischemia develop deposition of Aβ in the ventroposterior lateral and ventroposterior medial nuclei for as long as 9 months.[12] This might be similar with precious reports showing that statins reduced the production of Aβ in Alzheimer disease.[24] The mechanism of the reduction of Aβ by fluvastatin should be further investigated.

Thus, the rats treated with fluvastatin showed enhancement of angiogenesis and neurite outgrowth in the peri-infarct cortex and reduced deposition of Aβ in the ventrolateral–ventromedial thalamic nuclei. Because those regions are important sites for spatial learning,[25,26] we speculate that the enhancement of functional recovery by fluvastatin might be dependent on those regions.

The other histological difference was the reduction of superoxide anion in the ischemic core in fluvastatin-treated rats. Because cerebral blood flow in the ischemic cortex remained to be reduced for 48 hours and restored to some extent 9 days after permanent MCAo,[27] we speculate that fluvastatin could reach the ischemic core and show the antioxidative effects. On the contrary, in the peri-infarct region, superoxide anion was not detected even in the control group and no effect of fluvastatin might be observed. This effect of statin is similar with the previous report showing that cerivastatin prevented the production of superoxide anion in the cerebral parenchyma in stroke-prone spontaneously hypertensive rats.[28] Also, fluvastatin is reported to possess antioxidative properties in other cells.[29,30]

The association of neurogenesis is also the center of interest, because previous reports showed an increase in neurogenesis after atorvastatin treatment beginning at 1 day after stroke.[5] However, we speculate that neurogenesis might not have contributed to the favorable outcome in the present study, because the volume of infarction was not decreased by fluvastatin, and the density of mature neurons (NeuN-positive cells) and proliferative immature neurons (BrdU/DCX-positive cells) was the same in both groups. From the viewpoints, the timing of treatment seems important for the enhancement of neurogenesis and the beginning of statin 7 days after MCAo might be too late to enhance neurogenesis.

The limitation of the present study is that there is no data demonstrating that fluvastatin crossed over the blood–brain barrier and acted on neurons directly. Blood–brain barrier permeability differs among statins and correlates in part with their respective lipophilicity.[31] Considering that pretreatment with pravastatin and rosuvastatin, whose lipophilicity is 0.84 and 0.33, respectively, shows significant effects on reducing infarction volume,[31] fluvastatin, whose lipophilicity is 1.27, might penetrate blood–brain barrier and have some direct effects on neurons. Otherwise, fluvastatin could penetrate the brain because of the disruption of blood–brain barrier after MCAo. One of other limitations in the present study is no

examination of the characteristics of BrdU positive-cells other than CD31, DCX, or NeuN. In addition, how these histological changes in fluvastatin-treated rats were mechanistically linked to improved outcome was not clarified. Further study is necessary to clarify these points.

Summary

Overall, delayed postischemic chronic fluvastatin treatment showed beneficial effects on the recovery of cognitive impairment after stroke by enhancement of neuritogenesis and of angiogenesis and a decrease in Aβ deposition and superoxide anion production. Further studies might show potential clinical utility to treat cognitive impairment in patients with ischemic stroke.

Acknowledgments

The authors thank Dr Masatsugu Horiuchi and Dr Masaru Iwai for their helpful advice on superoxide detection by dihydroethidium staining, and Dr Hiroshi Sato for assistance with MRI.

Sources of Funding

This work was partially supported by a Grant-in-Aid from the Organization for Pharmaceutical Safety and Research, a Grant-in-Aid from The Ministry of Public Health and Welfare, a Grant-in-Aid from Japan Promotion of Science, and a Grant-in-Aid from the Ministry of Education, Culture, Sports, Science, and Technology, of the Japanese Government.

Disclosures

Fluvastatin was donated from Novartis Pharma. Masataka Sata received Honoraria payment (modest) from Novartis Pharma. Ryuichi Morishita received honoraria payment (modest) and has an advisory board relationship to Novartis Pharma.

References

1. Sacks FM, Pfeffer MA, Moye LA, Rouleau JL, Rutherford JD, Cole TG, Brown L, Warnica JW, Arnold JM, Wun CC, Davis BR, Braunwald E. The effect of pravastatin on coronary events after myocardial infarction in patients with average cholesterol levels: cholesterol and recurrent events trial investigators. *N Engl J Med*. 1996;335:1001–1009.
2. Amarenco P, Tonkin AM. Statins for stroke prevention: disappointment and hope. *Circulation*. 2004;109:III44–49.
3. Moonis M, Kane K, Schwiderski U, Sandage BW, Fisher M. HMG-CoA reductase inhibitors improve acute ischemic stroke outcome. *Stroke*. 2005;36:1298–1300.
4. Chen J, Zhang C, Jiang H, Li Y, Zhang L, Robin A, Katakowski M, Lu M, Chopp M. Atorvastatin induction of VEGF and BDNF promotes brain plasticity after stroke in mice. *J Cereb Blood Flow Metab*. 2005;25:281–290.
5. Chen J, Zhang ZG, Li Y, Wang Y, Wang L, Jiang H, Zhang C, Lu M, Katakowski M, Feldkamp CS, Chopp M. Statins induce angiogenesis, neurogenesis, and synaptogenesis after stroke. *Ann Neurol*. 2003;53:743–751.
6. Zhang L, Zhang ZG, Ding GL, Jiang Q, Liu X, Meng H, Hozeska A, Zhang C, Li L, Morris D, Zhang RL, Lu M, Chopp M. Multitargeted effects of statin-enhanced thrombolytic therapy for stroke with recombinant human tissue-type plasminogen activator in the rat. *Circulation*. 2005;112:3486–3494.
7. Belayev L, Alonso OF, Busto R, Zhao W, Ginsberg MD. Middle cerebral artery occlusion in the rat by intraluminal suture: neurological and pathological evaluation of an improved model. *Stroke*. 1996;27:1616–1623.
8. Sata M, Nishimatsu H, Osuga J, Tanaka K, Ishizaka N, Ishibashi S, Hirata Y, Nagai R. Statins augment collateral growth in response to ischemia but they do not promote cancer and atherosclerosis. *Hypertension*. 2004;43:1214–1220.
9. Nakatomi H, Kuriu T, Okabe S, Yamamoto S, Hatano O, Kawahara N, Tamura A, Kirino T, Nakatuku M. Regeneration of hippocampal pyramidal neurons after ischemic brain injury by recruitment of endogenous neural progenitors. *Cell*. 2002;110:429–441.
10. Petullo D, Masonic K, Lincoln C, Wibberley L, Teliska M, Yao DL. Model development and behavioral assessment of focal cerebral ischemia in rats. *Life Sci*. 1999;64:1099–1108.
11. Cavaglia M, Dombrowski SM, Drazba J, Vasanji A, Bokesch PM, Janigro D. Regional variation in brain capillary density and vascular response to ischemia. *Brain Res*. 2001;910:81–93.
12. van Groen T, Puurunen K, Maki HM, Sivenius J, Jolkkonen J. Transformation of diffuse beta-amyloid precursor protein and beta-amyloid deposits to plaques in the thalamus after transient occlusion of the middle cerebral artery in rats. *Stroke*. 2005;36:1551–1556.
13. Iwai M, Liu HW, Chen R, Ide A, Okamoto S, Hata R, Sakanaka M, Shiuchi T, Horiuchi M. Possible inhibition of focal cerebral ischemia by angiotensin II type 2 receptor stimulation. *Circulation*. 2004;110:843–848.
14. Robinson RG. Differential behavioral and biochemical effects of right and left hemispheric cerebral infarction in the rat. *Science*. 1979;205:707–710.
15. DeVries AC, Nelson RJ, Traystman RJ, Hurn PD. Cognitive and behavioral assessment in experimental stroke research: Will it prove useful? *Neurosci Biobehav Rev*. 2001;25:325–342.
16. Badan I, Platt D, Kessler C, Popa-Wagner A. Temporal dynamics of degenerative and regenerative events associated with cerebral ischemia in aged rats. *Gerontology*. 2003;49:356–365.
17. Badan I, Dinca I, Buchhold B, Suofu Y, Walker L, Gratz M, Platt D, Kessler CH, Popa-Wagner A. Accelerated accumulation of n- and c-terminal beta app fragments and delayed recovery of microtubule-associated protein 1b expression following stroke in aged rats. *Eur J Neurosci*. 2004;19:2270–2280.
18. Schabitz WR, Berger C, Kollmar R, Seitz M, Tanay E, Kiessling M, Schwab S, Sommer C. Effect of brain-derived neurotrophic factor treatment and forced arm use on functional motor recovery after small cortical ischemia. *Stroke*. 2004;35:992–997.
19. Endres M, Laufs U, Liao JK, Moskowitz MA. Targeting enos for stroke protection. *Trends Neurosci*. 2004;27:283–289.
20. Gonzalez-Billault C, Avila J, Caceres A. Evidence for the role of map1b in axon formation. *Mol Biol Cell*. 2001;12:2087–2098.
21. Pooler AM, Xi SC, Wurtman RJ. The 3-hydroxy-3-methylglutaryl co-enzyme a reductase inhibitor pravastatin enhances neurite outgrowth in hippocampal neurons. *J Neurochem*. 2006;97:716–723.
22. Wei L, Erinjeri JP, Rovainen CM, Woolsey TA. Collateral growth and angiogenesis around cortical stroke. *Stroke*. 2001;32:2179–2184.
23. Alexandrov AV, Hall CE, Labiche LA, Wojner AW, Grotta JC. Ischemic stunning of the brain: Early recanalization without immediate clinical improvement in acute ischemic stroke. *Stroke*. 2004;35:449–452.
24. Fassbender K, Simons M, Bergmann C, Stroick M, Lutjohann D, Keller P, Runz H, Kuhl S, Bertsch T, von Bergmann K, Hennerici M, Beyreuther K, Hartmann T. Simvastatin strongly reduces levels of Alzheimer's disease beta -amyloid peptides Abeta 42 and Abeta 40 in vitro and in vivo. *Proc Natl Acad Sci U S A*. 2001;98:5856–5861.
25. Casu MA, Wong TP, De Koninck Y, Ribeiro-da-Silva A, Cuello AC. Aging causes a preferential loss of cholinergic innervation of characterized neocortical pyramidal neurons. *Cereb Cortex*. 2002;12:329–337.
26. Jeljeli M, Strazielle C, Caston J, Lalonde R. Effects of ventrolateral-ventromedial thalamic lesions on motor coordination and spatial orientation in rats. *Neurosci Res*. 2003;47:309–316.
27. Rudin M, Baumann D, Ekatodramis D, Stimmann R, McAllister KH, Sauter A. MRI analysis of the changes in apparent water diffusion coefficient, t(2) relaxation time, and cerebral blood flow and volume in the temporal evolution of cerebral infarction following permanent middle cerebral artery occlusion in rats. *Exp Neurol*. 2001;169:56–63.
28. Kawashima S, Yamashita T, Miwa Y, Ozaki M, Namiki M, Hirase T, Inoue N, Hirata K, Yokoyama M. HMG-CoA reductase inhibitor has protective effects against stroke events in stroke-prone spontaneously hypertensive rats. *Stroke*. 2003;34:157–163.
29. Sumi D, Hayashi T, Thakur NK, Jayachandran M, Asai Y, Kano H, Matsui H, Iguchi A. A HMG-CoA reductase inhibitor possesses a potent anti-atherosclerotic effect other than serum lipid lowering effects–the relevance of endothelial nitric oxide synthase and superoxide anion scavenging action. *Atherosclerosis*. 2001;155:347–357.
30. Morita H, Saito Y, Ohashi N, Yoshikawa M, Katoh M, Ashida T, Kurihara H, Nakamura T, Kurabayashi M, Nagai R. Fluvastatin ameliorates the hyperhomocysteinemia-induced endothelial dysfunction: The antioxidative properties of fluvastatin. *Circ J*. 2005;69:475–480.
31. Endres M. Statins and stroke. *J Cereb Blood Flow Metab*. 2005;25:1093–1110.

JOURNAL OF NEUROTRAUMA
Volume 24, Number 6, 2007
© Mary Ann Liebert, Inc.
Pp. 1037–1054
DOI: 10.1089/neu.2006.0182

Intravenous Infusion of Dihydroginsenoside Rb1 Prevents Compressive Spinal Cord Injury and Ischemic Brain Damage through Upregulation of VEGF and Bcl-x_L

MASAHIRO SAKANAKA,[1] PENGXIANG ZHU,[1] BO ZHANG,[1] TONG-CHUN WEN,[1] FANG CAO,[1] YONG-JIE MA,[1] KEIICHI SAMUKAWA,[1] NORIAKI MITSUDA,[2] JUNYA TANAKA,[3] MAKOTO KURAMOTO,[4] HIDEMITSU UNO,[4] and RYUJI HATA[1]

ABSTRACT

Red ginseng root (Panax Ginseng CA Meyer) has been used clinically by many Asian people for thousands of years without any detrimental effects. One of the major components of Red ginseng root is ginsenoside Rb_1 (gRb1). Previously, we showed that intravenous infusion of gRb1 ameliorated ischemic brain damage through upregulation of an anti-apoptotic factor, Bcl-x_L and that topical application of gRb1 to burn wound lesion facilitated wound healing through upregulation of vascular endothelial growth factor (VEGF). In the present study, we produced dihydroginsenoside Rb1 (dgRb1), a stable chemical derivative of gRb1, and showed that intravenous infusion of dgRb1 improved spinal cord injury (SCI) as well as ischemic brain damage. As we expected, the effective dose of dgRb1 was ten times lower than that of gRb1. Intravenous infusion of dgRb1 at this effective dose did not affect brain temperature, blood pressure or cerebral blood flow, suggesting that dgRb1 rescued damaged neurons without affecting systemic parameters. In subsequent *in vitro* studies that focused on dgRb1–induced expression of gene products responsible for neuronal death or survival, we showed that dgRb1 could upregulate the expression of not only Bcl-x_L, but also a potent angiogenic and neurotrophic factor, VEGF. We also showed that dgRb1-induced expression of bcl-x_L and VEGF mRNA was HRE (hypoxia response element) and STRE (signal transducers and activators of transcription 5 (Stat5) response element) dependent, respectively.

Key words: Bcl-x_L; cerebral ischemia; ginsenoside Rb1; spinal cord injury; VEGF

INTRODUCTION

THE ANNUAL INCIDENCE of spinal cord injury (SCI) has been estimated to be approximately 20–40 persons per 1 million in the world (Profyris et al., 2004). The main causes of trauma to the cord are motor-vehicle accidents, sports and recreational activities, work-related accidents and falls at home. More importantly, the majority of SCI victims are young and otherwise healthy, and suffer the burden of life-long disability. At present, there is no universally accepted treatment for this pathological condition. Administration of methylprednisolone,

Departments of [1]Functional Histology, [2]Organ Physiology, and [3]Molecular and Cellular Physiology, Ehime University Graduate School of Medicine, Shitukawa, Toon, Ehime, Japan.
[4]Division of Synthesis and Analysis, Department of Molecular Science, Integrated Center for Sciences (INCS), Ehime University, Matsuyama, Japan.

surgical decompression of the spinal cord, and stabilization of the vertebrae of the spine are performed to prevent further injury. However, recovery from functional loss is limited (Enomoto et al., 2004).

Over the past several decades, researchers have been making desperate efforts, without any great success, searching for intravenously infusible neuroprotective agents for SCI. At present, only methylprednisolone is clinically available. However this agent, even though alleviating SCI, frequently causes serious adverse effects in humans by modulating inflammatory responses in an adverse manner (Sayer et al., 2006). Finding an intravenously infusible neuroprotective agent that acts safely and favorably on the damaged spinal cord tissue without an increased risk of infection or avascular necrosis of the femoral head appears to be a prerequisite for the treatment of SCI. We speculate that development of an intravenously infusible agent with a potent neuroprotective action would be of great value from the clinical point of view, because such an effective agent would greatly contribute to elucidation of the molecular mechanisms underlying the SCI for which the agent is applied, and would facilitate the development of other innovative treatment protocols and drugs.

Red ginseng root (Panax ginseng CA Meyer) is used clinically in Asian countries for various diseases, including atherosclerosis, liver dysfunction, cerebrovascular disease, hypertension and post-menopausal disorders (Kimura et al., 2006). Ginseng root consists of two major ingredients: crude ginseng saponin and crude ginseng non-saponin fractions. To date, more than 20 saponins have been isolated from ginseng root and identified chemically. They can be classified into three major groups according to their chemical structure: protopanaxadiol, protopanaxatriol and oleanolic acid saponins, of which ginsenoside Rb_1 (gRb1), ginsenoside Rg_1 and ginsenoside R_0 are respective representative substances (Shibata et al., 1994).

In our previous study, we showed that postischemic intravenous infusion of gRb1 ameliorated cortical infarct size, place navigation disability and secondary thalamic degeneration after permanent occlusion of the middle cerebral artery (MCA) in stroke-prone spontaneously hypertensive rats (SHR-SP), and demonstrated that gRb1 upregulated neuronal Bcl-x_L protein expression and prevented neuronal apoptosis *in vitro* and *in vivo* (Zhang et al., 2006). We also showed that topical application of gRb1 to burn wound ameliorated healing process through upregulation of the kerationocyte-derived vascular endothelial growth factor (VEGF) production *in vivo* and *in vitro* (Kimura et al., 2006). In the present study, we dehydrogenated gRb1 and produced dihydroginsenoside Rb1 (dgRb1, a stable chemical derivative of gRb1). We showed that intravenous infusion of dgRb1 improved SCI in rats, as well as ischemic brain damage in MCA-occluded rats. In subsequent *in vitro* experiments that focused on dgRb1–induced expression of gene products responsible for neuronal death or survival, we demonstrated that dgRb1 upregulated VEGF and Bcl-x_L expression and facilitated neuronal survival through hypoxia response element (HRE) and signal transducers and activators of transcription 5 response element (STRE), respectively.

METHODS

All experiments were approved by the Ethics Committee at Ehime University School of Medicine and were conducted according to the Guidelines for Animal Experimentation at Ehime University School of Medicine. Animals were housed in an animal room with a temperature range of 21–23°C and a 12-h light/dark cycle (light on: 7 a.m. to 7 p.m.). Animals were allowed access to food and water *ad libitum* until the end of the experiment.

Production and Purification of Dihydroginsenoside Rb1

Ginsenoside Rb1 (gRb1) was isolated and purified from the crude saponin fraction of the rhizome of Panax Ginseng C.A. Meyer (Zhang et al., 2006). Dihydroginsenoside Rb1 (dgRb1) was produced by the following method. First, 10% palladium charcoal (Pd/C) 10.2 mg was weighed, and placed in a two-necked flask with stop cocks. It was suspended by addition of methanol (GR) (1 mL). A hydrogen balloon (approximately 1.1 atom) was attached to the flask via one stop cock, and the other cock was connected to a vacuum pump. The catalyst (Pd/C) was activated at 0°C by several cycles of evacuation and agitation under hydrogen. After stirring for 30 min under hydrogen, ginsenoside Rb1 (19.9 mg) dissolved in methanol (1 ml) was injected into the flask through a syringe. The mixture was vigorously stirred at 0°C for 19.5 h using a magnetic stirrer. The reaction mixture was filtered through a filter paper and then a membrane filter with pores 0.45 μm in diameter. The product was dissolved in pure water (10 mL) and freeze-dried to obtain 19.1 mg dgRb1 (yield: 97%) as white powder. Then the product was purified by repeated column chromatography on silica gel with $CHCl_3$-MeOH-H_2O (65:35:10) and on ODS (octadecylsilyl) silica gel with MeOH-H_2O (1:1–7:3) (Samukawa et al., 1995). After purification, dihydrogenation of gRb1 was confirmed by ^{1}H-NMR. NMR spectra were obtained with a JNM-400 spectrometer, and ^{1}H chemical shifts were referenced to internal tetramethylsilane (0 ppm).

Osmotic Minipump Implantation

An osmotic minipump (model 2004 or 2001; Alza Corp., Palo Alto, CA) filled with either dgRb1 solution or vehicle (saline) was implanted subcutaneously in the back of each animal before ischemic or traumatic insult, and a fine silicon tube connected to the minipump was inserted into the left femoral vein after ischemic or traumatic insult.

Spinal Cord Injury in Wistar Rat

Adult male Wistar rats, aged 12–14 weeks, weighing 250–300 g, were used. Rats were anesthetized with 1.5% halothane in a 4:3 mixture of nitrous oxide and oxygen, and body temperature was kept at 37.0 ± 0.2°C during surgery. Spinal cord injury (SCI) was induced as described elsewhere (Morino et al., 2003). In brief, the back of the rat was shaved and disinfected. A longitudinal incision was made from the mid to low thoracic vertebrae. The dorsal surface of the spinal cord was exposed by laminectomy of the lower thoracic cord (Th12) vertebrae, and the dura was left intact. The exposed Th12 was compressed extradurally with a 20-g weight for 20 min. The muscles and skin were sutured with 4-0 silk. This method induces temporary paralysis of the lower extremities in a reproducible manner (Naruo et al., 2003). Thirty minutes later, a total of 60 μL of dgRb1 solution (1.2 or 6 μg/60 μL in saline) or the same volume of vehicle (saline) was infused once into the left femoral vein. Subsequently, continuous intravenous administration of dgRb1 was performed for 7 days using an osmotic minipump (1.2 or 6 μg/day). Control animals and sham-operated animals were administered with the same volume of physiological saline (vehicle).

Behavioral Evaluation after Spinal Cord Injury

As an open field test, a transparent acrylic box (30 × 30 × 30 cm) covered with a sound-attenuating shell (BOF-102; Biomedica, Osaka, Japan) was used. Inside the open field, an overhead incandescent bulb provided room lighting (approximately 110 lux), and a fan attached to the upper part of the box provided a masking noise of 45 dB. Animals were allowed to move freely in the open field for 20 min in the light condition. On each X and Y bank of the open field, infrared beams were attached 2 cm above the floor at 10-cm intervals, making a flip-flop circuit between the beams. The total number of circuit breaks was counted as the locomotor activity. On the X bank, 11 infrared beams were attached 12 cm above the floor at 2.5-cm intervals, and the total number of beam crossings was counted as the rearing activity. The open field locomotor scores (locomotor activity, rearing activity and BBB scores (Basso et al., 1995)) were measured before the loading of spinal cord injury, just after the loading of SCI, and from the 1st day to the 7th day after SCI, as indices of motor function. BBB scores of the sham-operated rats were 20–21.

Histological Observation and Quantitative Analysis of Spinal Cord Injury Damage

After evaluating behavioral performance, animals were anesthetized with an intraperitoneal injection of chloral hydrate (300 mg/kg) at 7 days after SCI and perfused transcardially with 0.1 M phosphate-buffered saline (pH 7.4) followed by perfusion with 500 ml of 4% paraformaldehyde in 0.1 M phosphate buffer (pH 7.4). The damaged spinal cords (1 cm in length) were dissected out. After fixation with the same fixative for overnight, each tissue sample was dehydrated, embedded in paraffin and sectioned in 5-μm increments. Each deparaffinized tissue section was treated with 10% non-immunized goat serum and incubated with a monoclonal antibody against microtubule-associated protein 2 (MAP2, SMI 52; Sternberger Monoclonals Inc., Lutherville, MD) for overnight at 4°C. After incubation with biotinylated anti-mouse IgG and peroxidase-conjugated streptavidin (DAKO A/S, Glostrup, Denmark), staining was visualized with 0.05% 3,3'-diaminobenzidine tetrahydrochloride and 0.01% hydrogen peroxide.

The separate animals (n = 5 in each group) were anesthetized with an intraperitoneal injection of chloral hydrate (300 mg/kg) at 7 days after SCI. The damaged spinal cords (1 cm in length) were dissected out. The samples were homogenized on ice with lysis buffer (0.5% SDS, 0.5% Triton-X, 100 μM phenylmethane sulfonyl fluoride, 20 μM Tris-HCl, pH 8.0). Then the samples were sonicated and centrifuged at 13,000 rpm for 10 min at 4°C. The protein content in the supernatant was determined using a BCA protein assay kit (Pierce, Rockland, IL). The supernatant was mixed with sample buffer (62.5mM Tris-HCl, pH 6.8, 2% sodium dodecylsulfate, 10% glycerol, and 0.001% bromophenol blue) to a final protein concentration of 1 mg/mL. Equal amounts of protein (15 μg) from the homogenates were electrophoresed and processed for immunoblot analysis using a monoclonal antibody against MAP2 (SMI 52, Sternberger Monoclonals Inc.). For semi-quantitative evaluation, the immunoreactive bands were subjected to densitometric analysis using a NIH Image program (National Institutes of Health, Bethesda, MD).

Middle Cerebral Artery Occlusion in Stroke-Prone Spontaneously Hypertensive Rats

Adult male SHR-SP rats, aged 12–14 weeks, weighing 250–300 g, were used. Rats were anesthetized with

1.5% halothane in a 4:3 mixture of nitrous oxide and oxygen, and brain temperature was maintained at 37.0 ± 0.2°C during surgery. The left MCA above the rhinal fissure and distal to the striate branches was coagulated and cut (Zhang et al., 2004).

Intravenous Infusion of dgRb1 after MCAO

DgRb1 was dissolved in isotonic saline. Then, 60 μL of dgRb1 solution (0.6 or 6 μg/60 μL) or the same volume of vehicle (saline) was injected into the left femoral vein of rats immediately after MCA occlusion, and then dgRb1 at a corresponding dose (0.6 or 6 μg/day, respectively) was continuously infused using an Alza osmotic minipump. MCA-occluded animals infused with saline were used as a control. The rate of continuous fluid infusion was 0.25 μL/h in all groups.

Measurement of Brain Temperature and Blood Pressure after MCAO

The brain temperature of rats with or without dgRb1 treatment was monitored by a combination of a temperature probe (XM-FH-BP 5 mm; Mini-Mitter Co., Sunriver, OR) inserted into the right cerebral hemisphere (1 mm anterior to the bregma, 1.5 mm lateral to the midline) and a telemetry system receiving signals from the probe (Data-Science Int., St. Paul, MN). The rats had free access to food and water except during the periods of minipump implantation and MCA occlusion (MCAO). The brain temperature was continuously monitored until the end of the experiment. The mean arterial blood pressure (MABP) in each animal was measured using a rat tail manometer-tachometer system (MK-1030, Muromachi Co., Tokyo, Japan).

TTC Staining 1 Day after MCAO

One day after MCAO, some animals were killed with an overdose of pentobarbital (50 mg/mL, 0.5 mL/animal) and decapitated. The brains were removed and sectioned coronally into 1-mm slices using a rat brain matrix (BRM-4000C; Activational System Inc., MI). Slices were immediately stained with 2% 2,3,5-triphenyltetrazolium chloride (TTC: Sigma, St. Louis, MO) and incubated at 37°C for 30 min. The border between infarcted and non-infarcted tissue was outlined with an image analysis system, and the area of infarction was measured by subtracting the area of the non-lesioned ipsilateral hemisphere from that of the contralateral hemisphere (Swanson et al., 1990). The volume of infarction was calculated by integration of the lesion areas at all equidistant levels of the forebrain.

Water Maze Test up to 4 Weeks after MCAO

The other MCA-occluded rats were subjected to repeated Morris water maze tests at 2 and 4 weeks after MCAO. Each test included three trials per day for 4 consecutive days. The rats were allowed to swim until they reached the submerged platform and to stay there for at least 10 sec. In the case that rats could not escape onto the platform within 90 sec, they were placed by hand onto the platform for 15 sec, and their escape latency was recorded as 90 sec. The mean latency of finding the invisible platform was measured for individual animals on each day.

Pathological Evaluation 4 Weeks after MCAO

After water maze tests, the animals were deeply anesthetized intraperitoneally with a lethal dose of sodium pentobarbital (50 mg/mL, 0.5 mL/animal), and perfused transcardially with 0.1 M phosphate-buffered saline (pH 7.4), followed by perfusion with 4% paraformaldehyde in 0.1M phosphate buffer (pH 7.4). The brain was dissected out and fixed in the same fixative. After taking a photograph of each brain, the infarcted region was traced on a sheet. Then the areas of the infarcted region and the left hemisphere of the brain were measured using a computerized processing system. The ratio of the infarcted area to the left hemispheric area was calculated.

Cortical Neuron Cultures

The cerebral cortices of 17-day-old rat embryos were aseptically dissected out. Cortical neurons were dissociated from the tissues as described elsewhere (Zhang et al., 2006). The dissociated cells were seeded on 24-well plastic plates (Corning, New York, NY) coated with poly-L-lysine, at a density of 5.0×10^5 cells/well.

SNP Treatment of Cultured Cortical Neurons

To induce apoptotic cell death, rat cortical neurons were exposed to 100 μM sodium nitroprusside (SNP, NO donor; Wako, Osaka, Japan) for 10 min. NO-induced neuronal death is characterized by nuclear fragmentation under electron microscopy and by DNA fragmentation as described elsewhere (Toku et al., 1998). Cortical neurons were cultured for 3 or 4 days *in vitro*, and then further cultured in the presence of $0–10^6$ fg/ml dgRb1 for 24 h, followed by SNP treatment for 10 min. After treatment, neurons were cultured for 16 h in Eagle's minimum essential medium (EMEM; Sigma) containing 1 mg/mL bovine serum albumin (BSA; Sigma) and 10mM HEPES (pH. 7.3; Invitrogen, Carlsbad, CA) with $0–10^6$ fg/mL dgRb1. Then, the neurons were homogenized and solubilized in Laemmli's sample solution containing 2% sodium dodecyl sulfate (Laemmli, 1970). An equal amount of protein (15 μg) from the homogenates was electrophoresed and processed for immunoblot analysis using a monoclonal antibody against MAP2 (SMI 52;

Sternberger Monoclonals Inc.). For semi-quantitative evaluation, the immunoreactive bands were subjected to densitometric analysis.

Analysis of VEGF and bcl-x_L mRNA Expression

Total RNA was extracted from cortical neurons cultured for 24 h with 0, 1, or 10^2 fg/mL dgRb1, using Isogen (Nippon Gene, Tokyo, Japan). It was then treated with DNase. Oligo dT primers together with 3 μg of DNase-treated total RNA and Moloney murine leukemia virus reverse transcriptase (Invitrogen, Carlsbad, CA) were used to obtain single strand DNA. PCR was conducted with the use of Takara EX Taq polymerase (Takara, Tokyo, Japan). The following conditions were used for PCR amplification: cDNA products of the reverse transcription reaction were denatured for 2 min at 94°C before 20 cycles (for β-actin), 35 cycles (for VEGF) or 25 cycles (for bcl-x_L) at 94°C for 1.5 min, 55°C for 1.5 min, and 72°C for 2 min. The RT-PCR products were separated on 3% agarose gel and visualized by ethidium bromide staining. The following pairs of oligonucleotides corresponding to certain sequences within the coding regions of the β-actin, VEGF and bcl-x_L genes were used as primers: rat β-actin primers; 5′ primer (5′-AGAAGAGCTATGAGCTGCCTGACG-3′), 3′ primer (5′-TACTTGCGCTCAGGAGGAGCAATG-3′); rat VEGF primers, 5′ primer (5′-CCATGAACTTTCTGCTCTCTTG-3′), 3′ primer (5′-GGTGAGAGGTCTAGTTCCCGA-3′); rat bcl-x_L primers, 5′ primer (5′-GTAGTGAATGAACTCTTTCGGGAT-3′), 3′ primer (5′-CCAGCCGCCGTTCTCCTGGATCCA-3′).

Analysis of VEGF and Bcl-x_L Protein Expression

Homogenates were obtained from cortical neurons cultured for 48 h with 0–10^6 fg/mL dgRb1. Homogenates were solubilized in Laemmli's sample solution containing 2% sodium dodecyl sulfate (Laemmli, 1970). An equal amount of protein (15 μg) from the homogenates was electrophoresed and processed for immunoblot analysis using mouse monoclonal antibodies against VEGF protein (Santa Cruz Biotech., Santa Cruz, CA) and Bcl-x_L protein (Transduction Laboratories Inc., Lexington, KY). For quantitative evaluation, the immunoreactive bands were subjected to densitometric analysis with NIH image software (National Institutes of Health, Bethesda, MD).

Construction of VEGF and Bcl-X Promoter Plasmids

The murine VEGF promoter fragment between positions −1106 and +113 relative to the transcription start site, was prepared by PCR with primers 5′-CCACGCTAGCGGGTAGGTTTGAATCACCATGCC-3′ and 5′-CCACAAGCTTAGTCCGCTGATAGTCTGCCTTG-3′. This segment, which contains the hypoxia response element (HRE), was inserted between the NheI and HindIII sites of the pGL2-basic vector (Promega, Madison, WI) to make the VEGF-wt plasmid. Mutation of the HRE element was generated by PCR using a sense primer (5′-TGCATACTCTGGTTTCCACAGGTCGTC-3′) and an antisense primer (5′-AAACCAGAGTATGCACTGTGTAGTCTGG-3′) carrying mutations, to make the VEGF-mut plasmid. The shorter promoter fragment between positions −755 and +113, which does not contain HRE, was also prepared by PCR with primers 5′-CCACGCTAGCAGATCAGACAAGGGCTCAGATAAG-3′ and 5′-CCACAAGCTTAGTCCGCTGATAGTCTGCCTTG-3′ and inserted between the NheI and HindIII sites of the pGL2-basic vector to make the VEGF-short plasmid.

The murine Bcl-X promoter fragment between positions -638 and -95 relative to the translation start site was prepared by PCR with primers 5′-CCACGAGCTCGATCTGGTCGATGGAGGAAC-3′ and 5′-AAACACCTGCTCACTTACTGGGTC-3′. This segment, which contains the Stat5 response element (STRE), was digested by SacI and BamHI, and inserted between the SacI and BamHI sites of the pGL2-basic vector to make the bcl-x-wt plasmid. Mutation in STRE was generated by PCR using a sense primer (5′-AGGCATTGAGGATAAAAGGG-3′) and an antisense primer (5′-CCCTTTTATCCTCAATGCCT-3′) carrying mutations, to make the bcl-x-mut plasmid. Another promoter fragment between positions -1217 and -592, which does not contain STRE, was also prepared by PCR with primers 5′-CGGCCCTCGAGCCCTGCAGGGGGCT-3′ and 5′-AATTGCGAAGCTTAGGAACCTGCC-3′, and inserted between the XhoI and HindIII sites of the pGL2-basic vector to make the bcl-x-0.6L plasmid (Silva et al., 1999).

Transient Transfection and Promoter Assays

Primary cultured neurons were seeded on 24-well PLL-coated plastic plates (5.0×10^5 cells/well). On the third day of culture, the cells were co-transfected with 0.4 μg of reporter plasmid and 0.1 μg of pRL-TK (Promega) internal control plasmid using Lipofectamine Plus Reagent (Invitrogen) according to the manufacturer's protocol. After transfection, the cells were incubated at 37°C. One day later, dgRb1 was added to the medium at a concentration of 100 fg/ml, and neurons were incubated for a further 24 h. The activities of firefly luciferase from promoter-luciferase plasmids and renilla luciferase from pRL-TK plasmid in the cell extracts were evaluated using a Dual-luciferase assay kit

(Promega) with a luminometer (TD-20/20; Turner Designs Inc., Sunnyvale, CA) according to the manufacturer's protocol.

Statistical Analysis

All values are presented as mean value ± SD. Statistical significance was tested by one-way analysis of variance (ANOVA) followed by Bonferroni's multiple comparison test. A p value less than 0.05 was considered to be statistically significant.

RESULTS

Characterization and Purity of dgRb1

The produced dgRb1 was confirmed to have purity of 99.999% or more as determined by high performance liquid chromatography (Fig. 1). After purification, dihydrogenation of gRb1 was confirmed by ^{1}H-NMR. The NMR charts of gRb1 and dgRb1 are shown in Figure 2. When we measured the NMR spectrum of gRb1, the vinylic proton appeared at 5.13 ppm as a broad triplet-like signal. Allylic methyl protons appeared at 1.62 and 1.68 ppm as two singlet signals, and the sugar C1 hemiacetal protons also appeared at 4.34, 4.42, 4.57, and 4.66 ppm as four doublet signals. On the other hand, when we measured the NMR spectrum of dgRb1, the vinylic proton signal disappeared and the methyl absorption shifted upward at 0.94 and 0.95 ppm as two doublet signals, because of disappearance of the double bond in the side chain by hydrogenation. The melting point of dgRb1 is 192–195°C, whereas that of gRb1 is 197–198°C (reference value).

Intravenous Infusion of dgRb1 Ameliorates Motor Deficit and Behavioral Abnormalities after Spinal Cord Injury in Rat

We first investigated the effects of intravenous infusion of dgRb1 on locomotor activity, rearing activity and BBB score in rats. All animals survived until the end of the experiment and exhibited motor deficit and behavioral abnormalities after SCI. Compared with the vehicle-treated group, the dgRb1–treated groups showed significant improvement of motor activity and behavioral abnormalities with respect to locomotor activity, rearing activity and BBB score in a dose dependent manner after SCI (Figs. 3A–C; $n = 8$ in each group).

Intravenous Infusion of dgRb1 Ameliorates Morphological Damage of the Spinal Cord after SCI in Rats

To evaluate morphological damage after SCI, we performed immuno-staining for MAP2. In the normal rat spinal cord, MAP2 immunoreactivity was localized predominantly in dendrites within the gray matter and white matter of the spinal cord (Fig. 4A). In the anterior horn of the damaged spinal cord at 7 days after SCI (Fig. 4B,C,D), chromatolytic neurons (Fig. 4F,H, arrowheads) and pigmented neurons (Fig. 4G,H, arrows) were detected while no such neurons were detected in the sham-operated control (Fig. 4E).

For quantitative analysis of SCI damage, we conducted western blot using an antibody against MAP2 protein. Compared with the saline-treated group, MAP2 protein expressions were clearly up-regulated in the spinal cords from the dgRb1–treated groups (Fig. 5A). Experiments were independently performed five times. Densitometric analysis of the immunoreactive bands revealed that compared with the saline-treated control, treatment with dgRb1 at the doses of 1.2 and 6.0 μg/day caused 2.0-fold and 2.2-fold increases in MAP2 protein expression in the rat damaged spinal cords, respectively (Fig. 5B).

Intravenous Infusion of dgRb1 Ameliorates Cortical Infarct Size and Place Navigation Disability in MCA-Occluded SHR-SP

We next investigated the effects of postischemic intravenous single infusion of dgRb1 on cortical infarct size in

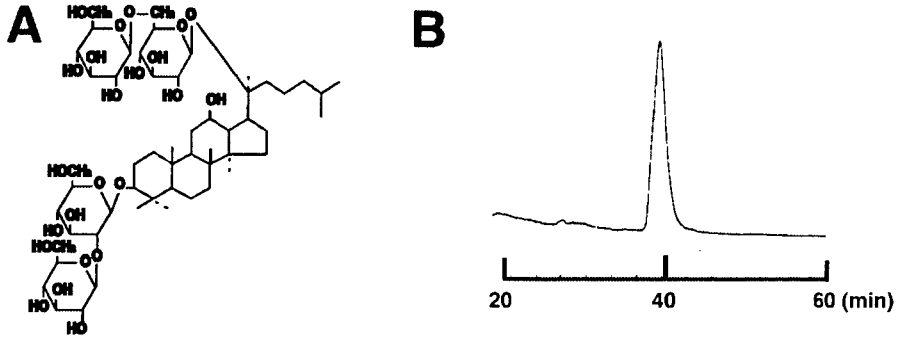

FIG. 1. (A) Chemical structure of dgRb$_1$. (B) HPLC purification of dgRb$_1$.

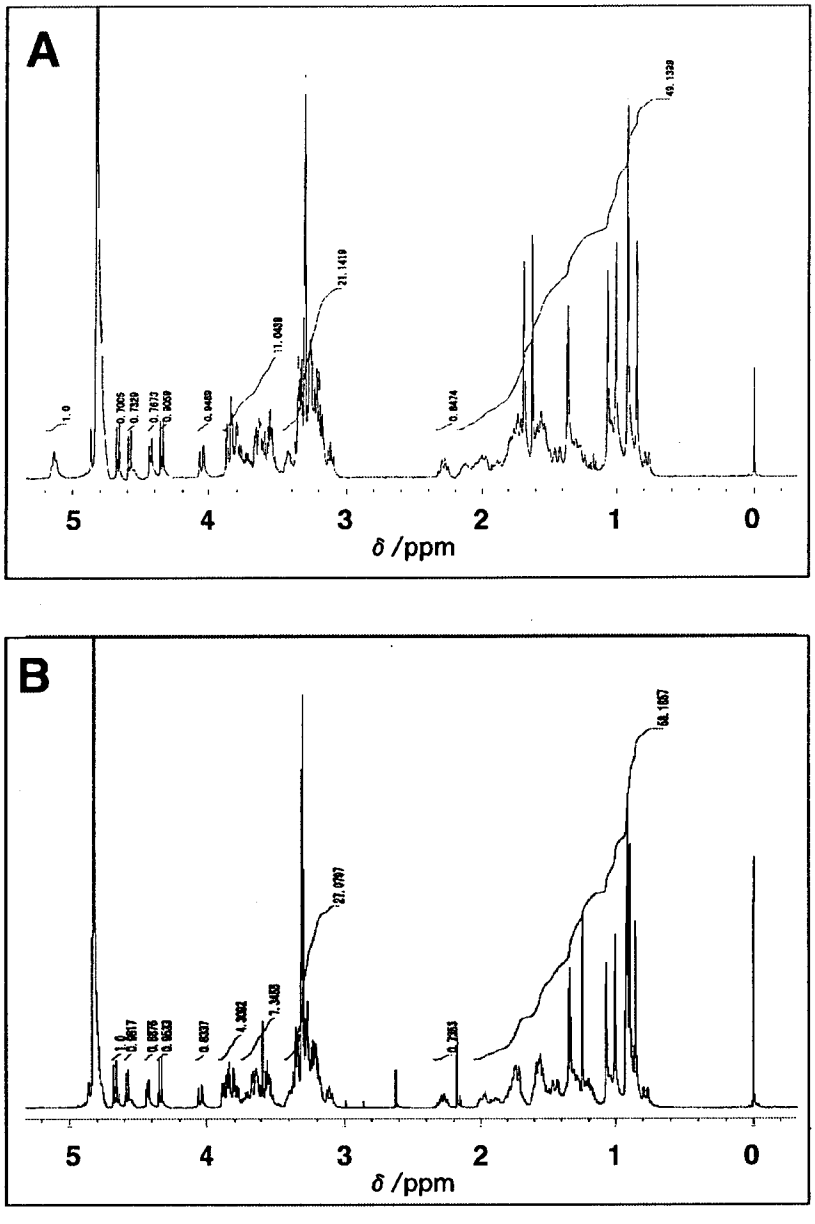

FIG. 2. 400-MHz ^{1}H-NMR spectra of ginsenoside Rb1(gRb1) and dihydroginsenoside Rb1(dgRb1) in CD_3OD. (**A**) 400-MHz ^{1}H-NMR spectrum of gRb1: the following characteristic signals were observed: a broad triplet-like signal due to the vinylic proton at 5.13 ppm, two singlet signals due to allylic methyl protons at 1.62 and 1.68 ppm, and four doublet signals due to the sugar C1 hemiacetal protons at 4.34, 4.42, 4.57, and 4.66 ppm. (**B**) 400-MHz ^{1}H-NMR spectrum of dgRb1: the vinylic proton signal has disappeared and the methyl absorptions have shifted upward at 0.94 and 0.95 ppm as two doublet signals due to disappearance of the double bond in the side chain by hydrogenation. The sugar parts are intact, since four sugar C1 hemiacetal protons are clearly observed at 4.38, 4.47, 4.62, and 4.71 ppm.

SHR-SP with permanent MCAO. All animals survived until the end of the experiment and exhibited cerebral infarction. TTC staining revealed significant reductions in total infarct volume and infarct area one day after middle cerebral artery occlusion (MCAO) (Fig. 6A,B). As shown in Figure 6B, total infarct volume in the dgRb1-treated groups (0.6 or 6 μg/day) became less than half that in the vehicle-treated group (saline; $n = 6$ in each group).

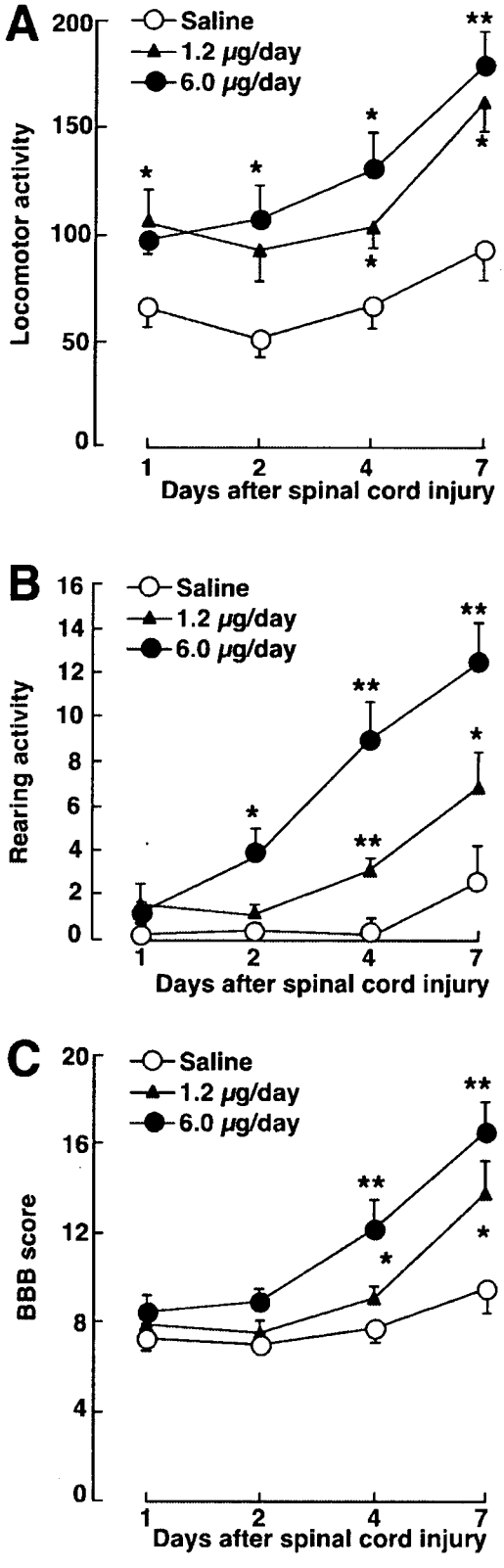

To confirm that the neuroprotective effects of dgRb1 lasted more than 4 weeks, we investigated the effects of postischemic continuous intravenous infusion of dgRb1 on cortical infarct size and place-navigation disability in SHR-SP at 4 weeks after permanent MCAO. When 0.6 or 6 μg/day of dgRb1 was intravenously infused after permanent MCAO for 4 weeks, the infarct area was markedly reduced in size (Fig. 7A,B). The proportion of infarct size in the groups treated with dgRb1 (0.6 or 6 μg/day) was significantly smaller than that in the vehicle-treated group (Fig. 7C; $n = 6$ in each group). Furthermore, postischemic intravenous infusion of dgRb1 at a dose of 0.6 or 6 μg/day significantly decreased the escape latency on repeated trials of the Morris water maze test, especially on the fourth trial day at 2 weeks after MCA occlusion (Fig. 7D) and on all 4 trial days at 4 weeks after MCA occlusion (Fig. 7E). There was no significant difference in swimming speed among the experimental groups (data not shown).

In addition, intravenous $dgRb_1$ infusion did not affect cerebral blood flow as monitored by laser Doppler flowmetry (Omega flow FLO-N1, Neuroscience Inc., Tokyo, Japan) (data not shown). Moreover, as shown in Table 1, there were no significant differences in MABP and brain temperature between the vehicle-treated group and dgRb1-treated group (6 μg/day; $n = 6$ in each group). These data suggest that the protective effect of dgRb1 on ischemic brain damage lasts at least 4 weeks and that intravenous infusion of dgRb1 has no noticeable systemic effect.

dgRb1 Prevents Apoptotic Neuron Death

To evaluate whether dgRb1, like gRb1, shows the anti-apoptotic action *in vitro*, we induced neuronal apoptosis by 10-min exposure of cultured neurons to the NO donor, sodium nitroprusside (SNP; 100 μM) with or without dgRb1 treatment (Zhang et al. 2006). The experiments were carried out independently five times. When cortical neurons were exposed to 100 μM SNP for 10 min, many of them underwent apoptosis within 16 h (Fig. 8A,B). On the other hand, when cortical neurons were incubated with 1, 100 or 10,000 fg/mL dgRb1 before, during and after SNP treatment, cell viability was maintained at a level close to that of control cortical neurons not exposed

FIG. 3. Intravenous infusion of dihydroginsenoside Rb1 (dgRb1) improved locomotor activity, rearing activity and BBB score after spinal cord injury (SCI) in Wistar rats. Note the significant improvement of locomotor activity, rearing activity and BBB score in dgRb1–treated rats ($n = 8$ in each group). *,**Significantly higher ($p < 0.05$, $p < 0.01$, respectively) than saline-treated control.

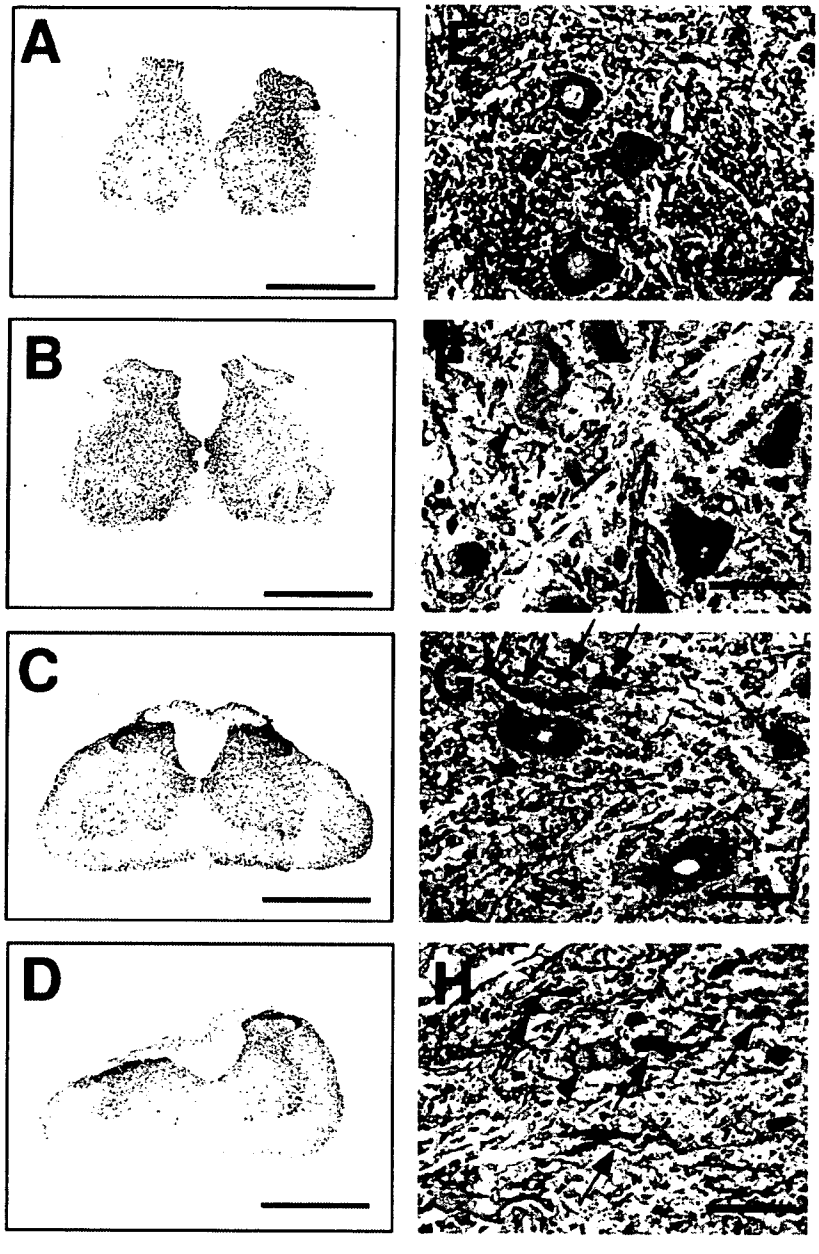

FIG. 4. Intravenous infusion of dihydroginsenoside Rb1 (dgRb1) ameliorates morphological damage of the spinal cord after spinal cord injury (SCI) in Wistar rats. (**A–D**) Representative photomicrographs of immuno-staining for MAP2 from the rat spinal cord at 7 days after SCI (A, sham; B, dgRb1(6.0 μg/day)–treated; C, dgRb1(1.2 μg/day)–treated; D, saline-treated). (**E–G**) Representative photomicrographs of immuno-staining for MAP2 in the anterior gray horn from the rat spinal cord at 7 days after SCI (E, sham; F, dgRb1(6.0 μg/day)–treated; G, dgRb1(1.2 μg/day)–treated; H, saline-treated). Scale bar = 1.0 mm (A–D), 50 μm (E–H). Note chromatolytic neurons (F,H, arrowheads) and pigmented neurons (G,H, arrows).

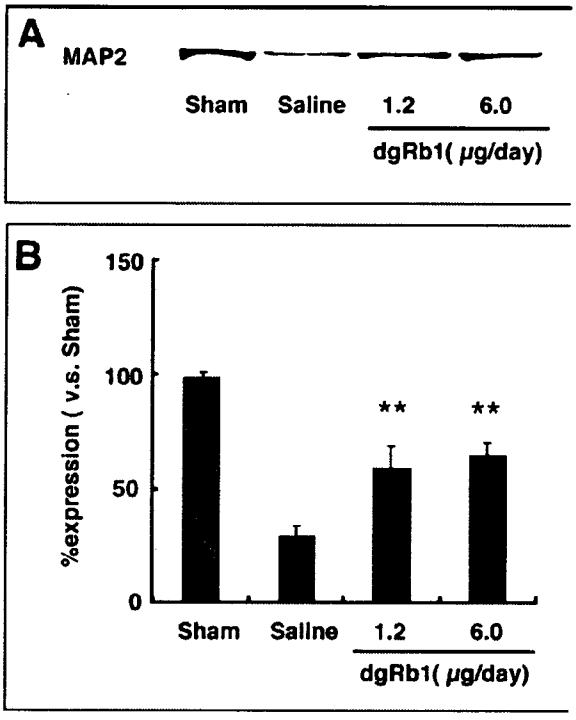

FIG. 5. Quantitative analysis of spinal cord injury (SCI) in Wistar rats. (A) Immunoblot analysis of MAP2 protein expression in the damaged spinal cords 7 days after SCI. (B) Densitometric analysis of MAP2-immunoreactive bands revealed that MAP2 protein expression in the damaged spinal cords from dihydroginsenoside Rb1 (dgRb1)–treated rats was significantly improved, compared with saline-treated control. Data were obtained from five independent experiments. **Significantly higher ($p < 0.01$) than saline-treated control.

to SNP (Fig. 8A,B). The anti-apoptotic action of dgRb1 implies that dgRb1 activates intracellular signaling to promote neuronal survival.

dgRb1 Upregulates Expression of Bcl-x_L and VEGF in Neurons

To gain an insight into the molecular mechanisms underlying dgRb1-mediated neuronal survival, we investigated dgRb1-induced changes in the expression of VEGF and bcl-x_L mRNA in neurons, using RT-PCR. RT-PCR using specific primers that amplify 496- and 628-bp fragments of rat VEGF mRNA and a 189-bp fragment of rat bcl-x_L mRNA detected PCR products of the expected sizes. Data were obtained from five independent experiments. As shown in Figure 9A,B, VEGF mRNA expression was upregulated significantly by treatment with dgRb1 at a concentration of 1 fg/mL for 24 h. Furthermore, bcl-x_L mRNA expression was also upregulated significantly by treatment with dgRb1 at concentrations of 1–100 fg/mL for 24 h (Fig. 9A,C).

In addition, we conducted western blot using an antibody against VEGF or Bcl-x_L protein. VEGF and Bcl-x_L proteins with molecular masses of approximately 26 and 29 kD, respectively were constitutively expressed in cultured neurons (Fig. 10A). Consistent with the increase in VEGF and bcl-x_L mRNA expression, both VEGF and Bcl-x_L protein expression were clearly upregulated in neurons cultured for 48 h in the presence of 1 or 100 fg/mL dgRb1 (Fig. 10A). Experiments were independently performed five times. Densitometric analysis of the immunoreactive bands revealed that treatment with dgRb1 at a concentration of 100 fg/mL caused a 2.1-fold

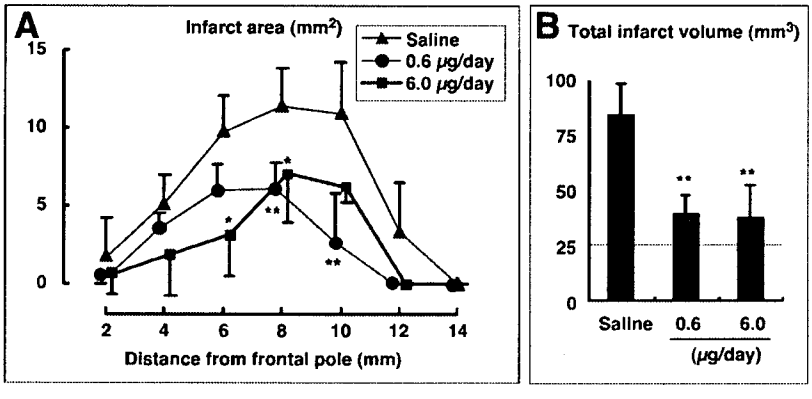

FIG. 6. Intravenous infusion of dihydroginsenoside Rb1(dgRb1) reduced cortical infarct size 24 h after permanent middle cerebral artery occlusion (MCAO) in stroke-prone spontaneously hypertensive rats (SHR-SP). Note that dgRb1 at doses of 0.6 and 6.0 μg/day significantly reduced the total infarct volume ($n = 6$ in each group). *,**Significantly lower ($p < 0.05$, $p < 0.01$, respectively) than saline-treated control.